Below we copied our responses to the reviewers' comments, which we already posted during the discussion phase. This is followed by the revised manuscript and supporting information, with the changes made highlighted in yellow.

Response to the comments made by Marcellus Ubbink:

We are grateful for the insightful comments and identifying errors.

Line 100: A 100-fold excess of TEV was used, that seems an awful lot for an enzyme. How was it removed? Was second NTA column used?

Response: We appreciate detection of this error! TEV protease was added in 0.1 molar ratio to remove the His_6 tag. In addition, a second 5 mL Ni-NTA column was used to remove the TEV protease from the protein. We propose to write in the revised manuscript: "the protein was dialysed into TEV protease buffer (50 mM Tris-HCl, pH 8.0, 300 mM NaCl and 1 mM beta-mercaptoethanol) to remove the His_6-tag by digestion with TEV protease overnight at 4 °C. His_6-tagged TEV protease was added in 0.1 molar ratio. The protease and cleaved His_6-tag were removed by running the sample again over a Ni-NTA column."

Lines 108, 109: The Bruker line of consoles is called Avance, not Advance

Response: Thank you for pointing out this typo, which will be corrected in the revised manuscript.

Table 1: It would be useful to add the number of PCS used in each calculation in an extra column. Also, the tensors for Tm3+ are very low indeed compared to those for Tb3+. Other tags, such as CLaNP give very high values for Tm3+ (~ 55 x 10^-32). Do the authors know why these differ so much? The Q-values are very low, as mentioned, and all but one are 0.03, yet looking at the plot for Ubi E16Q/E18Sep(Tm^{3+}) the spread looks clearly larger than for others (Fig. 2). How can that be?

Response: In the revised manuscript, we will replace Tables 1 and 2 in the main text as shown in the figures attached, with changes highlighted in yellow. All PCSs used for the tensor fits of the various ubiquitin and GB1 mutants are already listed in Tables S1 and S2, respectively.

Indeed, the difference in DeltaChi tensors obtained with Tm^{3+} and Tb^{3+} was larger than expected for the single-Sep mutants (but not for the GB1 mutant A24Sep/K28Sep). We observed previously that the ratio between the axial tensor components of these two ions can vary between different tags and even for the same tag at different sites of a protein (C.-T. Loh, B. Graham, E. H. Abdelkader, K. L. Tuck, G. Otting (2015) Generation of pseudocontact shifts in proteins with lanthanides using small "clickable" nitrilotriacetic acid and iminodiacetic acid tags *Chem. Eur. J.* 21, 5084-5092). These differences are not an artifact of fitting the tensors for Tm^{3+} and Tb^{3+} independently, as the fits yielded very similar coordinates for both metal ions. We do not understand the origin of these effects. It would help, if the effect of the ligand field could be predicted by quantum-mechanical calculations, but we were told by experts in the field that this is prohibitively difficult for lanthanide ions.

In the revised version, we propose to add the following paragraph in line 371:

"The DeltaChi tensors obtained with Tm^{3+} instead of Tb^{3+} ions were unexpectedly low for the single-Sep mutants, but not for the GB1 mutant A24Sep/K28Sep. We observed previously that the ratio between the DeltaChi_axial components of these two ions can vary between different tags and even for the same tag at different sites of a protein (Loh et al., 2015). These differences are not an artifact of fitting the tensors for Tm^{3+} and Tb^{3+} independently, as, with the exception of ubiquitin E18Sep, the fits converged to very similar metal positions (Tables 1 and 2). We do not understand the origin of different magnitudes of Chi-tensor anisotropies for Tm^{3+} and Tb^{3+} ions. In addition, much larger DeltaChi tensors have been reported for sterically rigid cyclen tags (Joss and Häussinger, 2019), suggesting that a rigid ligand field promotes large DeltaChi tensors."

The quality factor for the DeltaChi-tensor fit of Tb^{3+} in ubiquitin E18Sep differed from that of ubiquitin E16Q/E18Sep in the second digit, which was not displayed. On re-inspection, we noted that the *Q* factors had been rounded incorrectly: the *Q* factor for worse-fitting data should have been reported as 0.04 instead of 0.03. This was fixed in Table 1 attached and will be fixed in the revised version of the manuscript. In the case of Tm^{3+}, the back-calculated and experimental PCSs correlate similarly well in Fig. 2, and the *Q* factors were correspondingly similar.

Fig. S1: Can you indicate the fitted parameters for the ITC? Were n, Delta-H and K(D) all fitted? What are the results?

Response: The ITC measurements proved to be difficult. The data below are from three different measurements with Tb^{3+} and two different measurements with Tm^{3+}. The K_d values were derived from global fits. Fits were performed either with inclusion of the binding stoichiometry *n* as a fitting parameter or setting $n = 1$. Both results are included in the table attached. It is clear that these data do not yield the dissociation constant K_d with the accuracy suggested by the original manuscript. Therefore, we will change the sentence in line 145 to "Isothermal calorimetric experiments with Tb^{3+} and Tm^{3+} ions indicated dissociation constants of about 30–50 micromolar (Fig. S1)." and change the legend of Fig. S1 as shown in the attachment.

Response to the comments made by Claudio Luchinat:

We are grateful for the insightful comments and identifying errors.

Comment 1: The authors should comment that the axial anisotropies of the proposed tag attached to ubiquitin with a single phosphoserine mutation are significantly smaller than those of other previously proposed rigid tags (more than a factor 2 for Tb probes, more than a factor 5 for Tm), and should discuss the origin of this difference.

Response: The same point was picked up by Marcellus Ubbink and our response is copied here.

Indeed, the difference in DeltaChi tensors obtained with Tm^{3+} and Tb^{3+} was larger than expected for the single-Sep mutants (but not for the GB1 mutant A24Sep/K28Sep). We observed previously that the ratio between the axial tensor components of these two ions can

vary between different tags and even for the same tag at different sites of a protein (C.-T. Loh, B. Graham, E. H. Abdelkader, K. L. Tuck, G. Otting (2015) Generation of pseudocontact shifts in proteins with lanthanides using small "clickable" nitrilotriacetic acid and iminodiacetic acid tags *Chem. Eur. J.* 21, 5084-5092). These differences are not an artifact of fitting the tensors for Tm^{3+} and Tb^{3+} independently, as the fits yielded very similar coordinates for both metal ions. We do not understand the origin of these effects. It would help, if the effect of the ligand field could be predicted by quantum-mechanical calculations, but we were told by experts in the field that this is prohibitively difficult for lanthanide ions.

In the revised version, we propose to add the following paragraph in line 371:
"The DeltaChi tensors obtained with Tm^{3+} instead of Tb^{3+} ions were unexpectedly low for the single-Sep mutants, but not for the GB1 mutant A24Sep/K28Sep. We observed previously that the ratio between the DeltaChi_axial components of these two ions can vary between different tags and even for the same tag at different sites of a protein (Loh et al., 2015). These differences are not an artifact of fitting the tensors for Tm^{3+} and Tb^{3+} independently, as, with the exception of ubiquitin E18Sep, the fits converged to very similar metal positions (Tables 1 and 2). We do not understand the origin of different magnitudes of Chi-tensor anisotropies for Tm^{3+} and Tb^{3+} ions. In addition, much larger DeltaChi tensors have been reported for sterically rigid cyclen tags (Joss and Häussinger, 2019), suggesting that a rigid ligand field promotes large DeltaChi tensors."

Comment 2: The tensor for the GB1 K10D/T11Sep(Tb3+) should be reported with an axial component of -33.7 and a rhombic component of 14.7 to fulfill the axis labeling convention providing a rhombic component up to 2/3 of the axial component in absolute value. If the authors prefer to report the tensor as in Table 1, they should at least explain why. In any case, the tensor anisotropy is surprisingly large considering that the measured pcs span a range smaller than that measured for ubiquitin, and surprisingly rather rhombic. In the double phosphoserine K10Sep/T11Sep (Tb3+) mutant, the measured values of the pcs span a range which is roughly double, but the tensor is less than half with respect to that of K10D/T11Sep(Tb3+). Please, double check that no mix-up of data has occurred.

Response: Thank you for alerting us to this typo. The correct numbers for DelatChi_axial and DeltaChi_rhombic are 7.3 and 1.6, respectively.

Comment 3: Can you comment on the reason of the different sign of the tensor axial components between K10Sep/T11Sep(Tb3+) and A24Sep/K28Sep(Tb3+)? On the other hand, the sign of the axial components of Tb and Tm are usually opposite. Why are they the same in A24Sep/K28Sep.

Response: We do not understand the reason for the sign change in the tensor for Tb3+ between the K10Sep/T11Sep and A24Sep/K28Sep mutants. We double-checked and couldn't find an error. The signs were indeed wrong for the Tm3+ tensor associated with GB1 A24Sep/K28Sep(Tm3+): the correct values for the axial and rhombic components are -15.5 and -2.5, respectively.

In the revised version, we will display the isosurfaces also for Tm^{3+} in Figures 2, 3 and 4 to illustrate the degree of orthogonality of the tensors between Tm^{3+} and Tb^{3+} (revised Figures attached).

Comment 4: Minor points: Pag.2, line 1: “As lanthanide ions display particularly large. . .” not all lanthanoids, only some of them! Pag. 2, line 2: “While paramagnetic lanthanide ions generate paramagnetic relaxation enhancements (PRE) in the protein irrespective of metal mobility” This sentence may be read that PREs do not depend on mobility, which is slightly inaccurate, because internal mobility changes the correlation time of dipole-dipole relaxation (see Fragai et al. Coord. Chem. Rev. 2013, 257, 2652 for a thorough discussion). Please, clarify this point. Caption to Fig. 3: please indicate all panel letters.

Response: In the revised version, we propose the following changes.

Page 2, line 1: “As many lanthanide ions display particularly large…”

Page 2, paragraph 2: “Paramagnetic lanthanide ions always generate paramagnetic relaxation enhancements (PRE) in the protein, which vary relatively little with minor movements of the metal ion. In contrast, PCSs can decrease dramatically if the lanthanide complex reorientates relative to the protein.”

Response to the comments made by Claudio Luchinat:

We are grateful for the insightful comments and identifying errors.

Comment 1: The authors should comment that the axial anisotropies of the proposed tag attached to ubiquitin with a single phosphoserine mutation are significantly smaller than those of other previously proposed rigid tags (more than a factor 2 for Tb probes, more than a factor 5 for Tm), and should discuss the origin of this difference.

Response: The same point was picked up by Marcellus Ubbink and our response is copied here.

Indeed, the difference in DeltaChi tensors obtained with Tm^{3+} and Tb^{3+} was larger than expected for the single-Sep mutants (but not for the GB1 mutant A24Sep/K28Sep). We observed previously that the ratio between the axial tensor components of these two ions can vary between different tags and even for the same tag at different sites of a protein (C.-T. Loh, B. Graham, E. H. Abdelkader, K. L. Tuck, G. Otting (2015) Generation of pseudocontact shifts in proteins with lanthanides using small "clickable" nitrilotriacetic acid and iminodiacetic acid tags *Chem. Eur. J.* 21, 5084-5092). These differences are not an artifact of fitting the tensors for Tm^{3+} and Tb^{3+} independently, as the fits yielded very similar coordinates for both metal ions. We do not understand the origin of these effects. It would help, if the effect of the ligand field could be predicted by quantum-mechanical calculations, but we were told by experts in the field that this is prohibitively difficult for lanthanide ions.

In the revised version, we propose to add the following paragraph in line 371:
“The DeltaChi tensors obtained with Tm^{3+} instead of Tb^{3+} ions were unexpectedly low for the single-Sep mutants, but not for the GB1 mutant A24Sep/K28Sep. We observed previously that the ratio between the DeltaChi_axial components of these two ions can vary between different tags and even for the same tag at different sites of a protein (Loh et al., 2015). These differences are not an artifact of fitting the tensors for Tm^{3+} and Tb^{3+} independently, as, with the exception of ubiquitin E18Sep, the fits converged to very similar metal positions (Tables 1 and 2). We do not understand the origin of different magnitudes of Chi-tensor anisotropies for Tm^{3+} and Tb^{3+} ions. In addition, much larger DeltaChi tensors have been reported for sterically rigid cyclen

tags (Joss and Häussinger, 2019), suggesting that a rigid ligand field promotes large DeltaChi tensors."

Comment 2: The tensor for the GB1 K10D/T11Sep(Tb3+) should be reported with an axial component of -33.7 and a rhombic component of 14.7 to fulfill the axis labeling convention providing a rhombic component up to 2/3 of the axial component in absolute value. If the authors prefer to report the tensor as in Table 1, they should at least explain why. In any case, the tensor anisotropy is surprisingly large considering that the measured pcs span a range smaller than that measured for ubiquitin, and surprisingly rather rhombic. In the double phosphoserine K10Sep/T11Sep (Tb3+) mutant, the measured values of the pcs span a range which is roughly double, but the tensor is less than half with respect to that of K10D/T11Sep(Tb3+). Please, double check that no mix-up of data has occurred.

Response: Thank you for alerting us to this typo. The correct numbers for DelatChi_axial and DeltaChi_rhombic are 7.3 and 1.6, respectively.

Comment 3: Can you comment on the reason of the different sign of the tensor axial components between K10Sep/T11Sep(Tb3+) and A24Sep/K28Sep(Tb3+)? On the other hand, the sign of the axial components of Tb and Tm are usually opposite. Why are they the same in A24Sep/K28Sep.

Response: We do not understand the reason for the sign change in the tensor for Tb3+ between the K10Sep/T11Sep and A24Sep/K28Sep mutants. We double-checked and couldn't find an error. The signs were indeed wrong for the Tm3+ tensor associated with GB1 A24Sep/K28Sep(Tm3+): the correct values for the axial and rhombic components are -15.5 and -2.5, respectively.

In the revised version, we will display the isosurfaces also for Tm^{3+} in Figures 2, 3 and 4 to illustrate the degree of orthogonality of the tensors between Tm^{3+} and Tb^{3+} (revised Figures attached).

Comment 4: Minor points: Pag.2, line 1: "As lanthanide ions display particularly large. . ." not all lanthanoids, only some of them! Pag. 2, line 2: "While paramagnetic lanthanide ions generate paramagnetic relaxation enhancements (PRE) in the protein irrespective of metal mobility" This sentence may be read that PREs do not depend on mobility, which is slightly inaccurate, because internal mobility changes the correlation time of dipole-dipole relaxation (see Fragai et al. Coord. Chem. Rev. 2013, 257, 2652 for a thorough discussion). Please, clarify this point. Caption to Fig. 3: please indicate all panel letters.

Response: In the revised version, we propose the following changes.

Page 2, line 1: "As many lanthanide ions display particularly large…"

Page 2, paragraph 2: "Paramagnetic lanthanide ions always generate paramagnetic relaxation enhancements (PRE) in the protein, which vary relatively little with minor movements of the metal ion. In contrast, PCSs can decrease dramatically if the lanthanide complex reorientates relative to the protein."

Phosphoserine for the generation of lanthanide binding sites on proteins for paramagnetic NMR

Sreelakshmi Mekkattu Tharayil[1,*], Mithun Chamikara Mahawaththa[1,*], Choy-Theng Loh[1,2], Ibidolapo Adekoya[1], Gottfried Otting[1]

[1] ARC Centre of Excellence for Innovations in Peptide and Protein Science, Research School of Chemistry, Australian National University, Canberra ACT 2601, Australia

[2] present address: Hangzhou Wayland Bioscience Co. Ltd, Hangzhou 310030, PR China

[*] The first two authors contributed equally.

Correspondence to: Gottfried Otting (gottfried.otting@anu.edu.au)

Abstract. Pseudocontact shifts (PCS) generated by paramagnetic lanthanide ions provide valuable long-range structural information in NMR spectroscopic analyses of biological macromolecules such as proteins, but labelling proteins site-specifically with a single lanthanide ion remains an ongoing challenge, especially for proteins that are not suitable for ligation with cysteine-reactive lanthanide complexes. We show that a specific lanthanide binding site can be installed on proteins by incorporation of phosphoserine in conjunction with other negatively charged residues, such as aspartate, glutamate or a second phosphoserine residue. The close proximity of the binding sites to the protein backbone leads to good immobilization of the lanthanide ion, as evidenced by the excellent quality of fits between experimental PCSs and PCSs calculated with a single magnetic susceptibility anisotropy ($\Delta\chi$) tensor. An improved two-plasmid system was designed to enhance the yields of proteins with genetically encoded phosphoserine and good lanthanide ion affinities were obtained when the side chains of the phosphoserine and aspartate residues are not engaged in salt bridges, although the presence of too many negatively charged residues in close proximity can also lead to unfolding of the protein. In view of the quality of the $\Delta\chi$ tensors that can be obtained from lanthanide binding sites generated by site-specific incorporation of phosphoserine, this method presents an attractive tool for generating PCSs in stable proteins, particularly as it is independent of cysteine residues.

1 Introduction

Paramagnetic labels offer an attractive tool for the study of protein structure and function, as the magnetic moments of unpaired electrons generate long-range paramagnetic effects in NMR spectra. Among the paramagnetic effects that can be observed in NMR spectra, pseudocontact shifts (PCS) generated by paramagnetic metal ions stand out for their high information content and ease of observation (Otting, 2008; Parigi and Luchinat, 2018). Specifically, the PCSs provide information about the location of nuclear spins relative to the magnetic susceptibility anisotropy tensor ($\Delta\chi$ tensor) associated with a paramagnetic metal ion, and this information can readily be obtained for nuclear spins as far as 40 Å from the paramagnetic centre (Bertini et al., 2001).

As many lanthanide ions display particularly large $\Delta\chi$ tensors (Bleaney, 1972; Bertini et al., 2001), significant efforts have been made to devise lanthanide complexes for site-specific tagging of proteins (Su and Otting, 2010; Keizers and Ubbink, 2011; Nitsche and Otting, 2017; Joss and Häussinger, 2019; Saio and Ishimori, 2020). In an alternative approach, PCSs can be elicited in proteins by creating binding sites for lanthanides or lanthanide complexes by protein engineering (Yagi et al., 2010; Barthelmes et al., 2011, 2015; Jia et al., 2011).

A common problem of lanthanide tags arises from mobility of the metal-ion complex relative to the target protein. Paramagnetic lanthanide ions always generate paramagnetic relaxation enhancements (PRE) in the protein, which vary relatively little with minor movements of the metal ion. In contrast, PCSs can decrease dramatically if the lanthanide complex reorientates relative to the protein. With a limited degree of tag flexibility, the PCSs may still be explained by a single effective $\Delta\chi$ tensor although, in principle, a family of $\Delta\chi$ tensors would be required to account for multiple tag conformations (Shishmarev and Otting, 2013). Well immobilized metal ions thus not only deliver larger PCSs but also more reliable $\Delta\chi$-tensor fits.

Different strategies have been devised to immobilise lanthanide ions on proteins. Tag motions can be restricted by short tethers and bulky lanthanide complexes to hem in the tag sterically (Nitsche and Otting, 2017). Double-arm tags provide two attachment points (Keizers and Ubbink, 2011), but even these designs have shown signs of tag mobility (Hass et al., 2010). A lanthanide-binding peptide (LBP) engineered into polypeptide loops of protein structures can deliver good metal immobilization but presents a major modification of the target protein (Barthelmes et al., 2011; 2017). Fusions of an LBP combined with disulfide bond formation have also been explored, but do not necessarily achieve good immobilisation of the lanthanide ion (Saio et al., 2009, 2010, 2011). A successful strategy has been a design, where two neighbouring cysteine residues are furnished with metal chelating tags and a single lanthanide ion is coordinated by both chelating groups (Swarbrick et al., 2011; Welegedara et al., 2017), a design that has also proven successful for Co^{2+} ions (Swarbrick et al., 2016). The most serious drawback of this design is its reliance on cysteine residues, which makes it incompatible with proteins that contain functionally important cysteine residues in their wild-type sequence. In fact, most of the currently available lanthanide tags target cysteines (Su and Otting, 2010; Keizers and Ubbink, 2011; Nitsche and Otting, 2017; Joss and Häussinger, 2019; Saio and Ishimori, 2020), as thiol groups can readily undergo selective chemical reactions. To avoid the mobility of solvent-exposed cysteine side chains, tags have also been designed for attachment to the side chains of aromatic residues, which are more hindered sterically and thus discouraged from populating different rotamers (Loh et al., 2015; Abdelkader et al., 2016), but this approach results in long linkers between the lanthanide ion and the protein, increasing the chances that the lanthanide ion moves and reorientates relative to the protein backbone.

The most elegant strategy for generating a lanthanide binding site in a protein would be to introduce a lanthanide-binding unnatural amino acid that can be site-specifically incorporated by genetic encoding. This approach would relieve any reliance on cysteine residues. Although systems for genetic encoding have been devised for over 100 different unnatural amino acids, only few of these can bind metal ions (Dumas et al., 2014) and those that do were found to precipitate proteins upon binding lanthanide ions. For example, protein precipitation has been reported for 2-amino-3-(8-hydroxyquinolin-3-yl)

propanoic acid (HQ-Ala; Jones et al., 2009) and we found ourselves incapable of improving on these results. Similarly, bipyridyl-alanine (Bpa) was shown to allow binding of Co^{2+} and the observation of PCSs (Nguyen et al., 2011), but subsequent experiments with Bpa incorporated in different proteins and at different sites showed that also this system is prone to precipitating proteins upon addition of metal ion.

In the present work, we explored the potential of a different unnatural amino acid, phosphoserine (Sep), to create a lanthanide binding site. Lanthanide ions are known for their affinity to negatively charged oxygens and, with a pK_a value of 5.6 for the equilibrium between monobasic and dibasic forms (Xie et al., 2005), a phosphoserine residue carries two negative charges under physiological conditions. Phosphorylation of serine residues is a well-known posttranslational modification of proteins effected by kinases, but this often is neither quantitative nor easily achievable for specific serine residues. Recently, however, an orthogonal phosphoseryl-tRNA-synthetase/tRNA pair has become available, which allows installing a Sep residue in response to an amber stop codon (Lee et al., 2013; Pirman et al., 2015; Yang et al., 2016). In the following we show that the system is sufficiently effective to install two Sep residues in the same protein, explore the potential to create a lanthanide binding site using a Sep residue in conjunction with other negatively charged residues, in particular an aspartate or a second Sep residue, and demonstrate the exceptional quality of $\Delta\chi$ tensors that can be obtained with lanthanide ions in these sites.

2 Experimental procedures

2.1 Plasmid preparation for protein expression

The plasmid SepOTSλ, which contains the phosphoseryl-tRNA synthetase/tRNA pair and a suitable EF-Tu mutant for incorporation of Sep in response to an amber stop codon (Pirman et al., 2015), was obtained from Addgene. To create a T7 expression vector that is compatible with SepOTSλ, we subcloned the region containing the T7 promoter, ribosome binding site, multiple cloning site and T7 terminator from pETMCSIII (Neylon et al., 2000) into the plasmid pCDF (Lammers et al., 2014). The gene of interest was inserted into the multiple cloning site and furnished with a C-terminal His_6-tag preceded by a TEV cleavage site. All plasmid constructions were conducted with a QuikChange protocol using mutant T4 DNA polymerase (Qi and Otting, 2019).

2.2 Protein expression

All proteins were expressed in the BL21ΔserB strain (Park et al., 2011), which lacks phosphoserine phosphatase and thus minimizes the dephosphorylation of phosphoserine to serine. The SepOTSλ and pCDF plasmids were co-transformed into electrocompetent BL21ΔserB cells. In order to minimize usage of amino acids and $^{15}NH_4Cl$, the following top-down expression method was used. Initially, 1 litre of cell-culture was grown in LB medium with 25 μM spectinomycin and 20 μM kanamycin at 37 °C until the OD_{600} value reached 0.6–0.8. Next, the cells were pelleted and resuspended in 300 mL M9 medium (6 g L^{-1}

Na_2HPO_4, 3 g L^{-1} KH_2PO_4, 0.5 g L^{-1} NaCl) and supplied with 1 g L^{-1} $^{15}NH_4Cl$ and 1 mM phosphoserine. Subsequently, the cells were incubated for 30 minutes at 37 °C and induced with IPTG. Protein expression was conducted at 25 °C overnight. Cells were harvested by centrifugation at 5,000 *g* for 15 minutes and lysed by passing twice through a French Press (SLM Amicon, USA) at 830 bars. The lysate was then centrifuged at 13,000 *g* for 60 minutes and the filtered supernatant was loaded onto a 5 mL Ni-NTA column (GE Healthcare, USA) equilibrated with binding buffer (50 mM Tris-HCl, pH 7.5, 300 mM NaCl, 5 % glycerol). The protein was eluted with elution buffer (binding buffer containing, in addition, 300 mM imidazole). For the double-amber mutants, the protein was dialysed into TEV protease buffer (50 mM Tris-HCl, pH 8.0, 300 mM NaCl and 1 mM β-mercaptoethanol) to remove the His_6-tag by digestion with TEV protease overnight at 4 °C. His_6-tagged TEV protease was added in 0.1 molar ratio. The protease and cleaved His_6-tag were removed by running the sample again over a Ni-NTA column. The resulting protein samples were then treated with 5 mM EDTA to remove any di- or trivalent metal ion that could have been adsorbed during protein expression and purification. Finally, EDTA was removed by buffer exchange with NMR buffer (20 mM HEPES-KOH, pH 7.0) using a HiPrep desalting column (GE Healthcare, USA). Mass-spectrometric analysis was conducted using an Elite Hybrid Ion Trap-Orbitrap mass spectrometer (Thermo Scientific, USA) coupled with an UltiMate S4 3000 UHPLC (Thermo Scientific, USA). 7.5 pmol of sample were injected to the mass analyser via an Agilent ZORBAX SB-C3 Rapid Resolution HT Threaded Column (Agilent, USA).

2.3 NMR spectroscopy

All NMR spectra were recorded at 25 °C, using an 800 MHz Bruker Avance NMR spectrometer for all mutants containing a single phosphoserine residue and a 600 MHz Bruker Avance NMR spectrometer for all mutants containing two phosphoserine residues. Samples were prepared in 20 mM HEPES buffer, pH 7.0, in 3 mm NMR tubes. 10 % D_2O was added to provide a lock signal. 0.1– 0.5 mM protein samples were used for 2D [^{15}N,^{1}H]-HSQC experiments. Complexes with lanthanides were obtained by titration with 10 mM $LnCl_3$ stock solutions.

2.4 PCS measurements and Δχ-tensor fitting

Pseudocontact shifts (PCS) were measured in ppm as the difference in amide proton chemical shift between the paramagnetic and diamagnetic NMR spectrum. PCSs were used to determine the position and orientation of the Δχ-tensor of the paramagnetic ions relative to the protein structure. Fitting of Δχ tensors was performed using the program Paramagpy (Orton et al., 2020).

2.5 Isothermal titration calorimetry

Isothermal calorimetric titration experiments were performed using a Nano-ITC low volume calorimeter (TA Instruments, USA) at 25 °C with stirring at 250 rpm. The protein mutant E18Sep and the titrants $TbCl_3$ and $TmCl_3$ were prepared in the same buffer (20 mM HEPES, pH 7.0) and degassed before use. Data were analysed using the programs NITPIC and SEDPHAT (Keller et al., 2012). The baseline-subtracted power peaks were integrated, and the integrated heat values fitted to the single binding site model (A + B ↔ AB, heteroassociation) to obtain the dissociation constant (K_d). The global fitting was done by repeatedly cycling between Marquardt–Levenberg and Simplex algorithms in SEDPHAT until modelling parameters converged; 68 % confidence intervals were calculated using the automatic confidence interval search with the projection method using F-statistics in SEDPHAT.

3 Results

3.1 Phosphoserine incorporation

Simultaneous transfection of *E. coli* with the SepOTSλ plasmid and pET vectors containing the genes of proteins targeted for overexpression and Sep incorporation led to slow cell growth and variable colony sizes on plates as described earlier (Pirman et al., 2015). Noting that the SepOTSλ plasmid contains the origin of replication of pUC, which belongs to the same plasmid incompatibility group as pET vectors (Morgan, 2014), we constructed a new expression vector based on pCDF to include T7 promoter, ribosome binding site, multiple cloning site and T7 terminator. This modification restored the usual growth rates of the cells. Proteins containing phosphoserine were expressed from a two-plasmid system containing SepOTSλ and a modified pCDF vector in BL21ΔserB. Expression yields of up to 3 mg purified protein per litre of growth medium were obtained.

3.2 Single phosphoserine residues for lanthanide binding

We used the proteins ubiquitin and GB1 to test whether a single phosphoserine residue is sufficient to create a lanthanide binding site. We hypothesized that a phosphoserine residue assisted by an additional carboxy group from a glutamate or aspartate residue (in the following referred to as 'helper residue') could potentially be sufficient to generate a tridentate complex with a lanthanide ion, positioning the metal ion close to the protein backbone and compensating its positive charge. In the first example, we made the mutant E18Sep of ubiquitin, where E16 and D21 could act as potential helper residues. Subsequent titration with Tb^{3+} ions succeeded in generating PCSs of up to almost 1 ppm (Table S1). The paramagnetic peaks appeared at chemical shifts different from the diamagnetic parent peaks, indicating slow exchange between lanthanide-bound and free protein. Isothermal calorimetric experiments with Tb^{3+} and Tm^{3+} ions indicated dissociation constants of about 30–50 µM (Fig. S1).

Figure 1a shows the PCSs observed with Tb^{3+} and Tm^{3+} ions after addition in equimolar ratio. Using the NMR ensemble structure of ubiquitin (PDB ID: 2KOX; Fenwick et al., 2011) and the measured PCSs, the metal position was

determined by fitting the Δχ tensor using the program Paramagpy (Table 1; Orton et al., 2020). The correlation between back-calculated and experimental PCSs was excellent (Fig. 2a, Table S1), resulting in *Q* factors lower than 0.04. This indicated that the Sep residue and lanthanide complex did not alter the structure of the protein. Furthermore, the tensor fit positioned the lanthanide ion between the phosphoserine residue and D21, suggesting that D21 acts as a helper residue rather than E16. To verify this result, we prepared the two ubiquitin mutants E18Sep/E16Q and E18Sep/D21N. As expected, the former delivered similar PCSs (Fig. 1b, Table S1), a similarly good Δχ-tensor fit (Table 1) and a similar metal position, whereas the latter showed only very small chemical shift changes upon titration with lanthanides, indicating a faster exchange (Fig. 1c). The paramagnetic centre identified by the fits placed the lanthanide ions between the aspartate and Sep residues as expected (Fig. 2b).

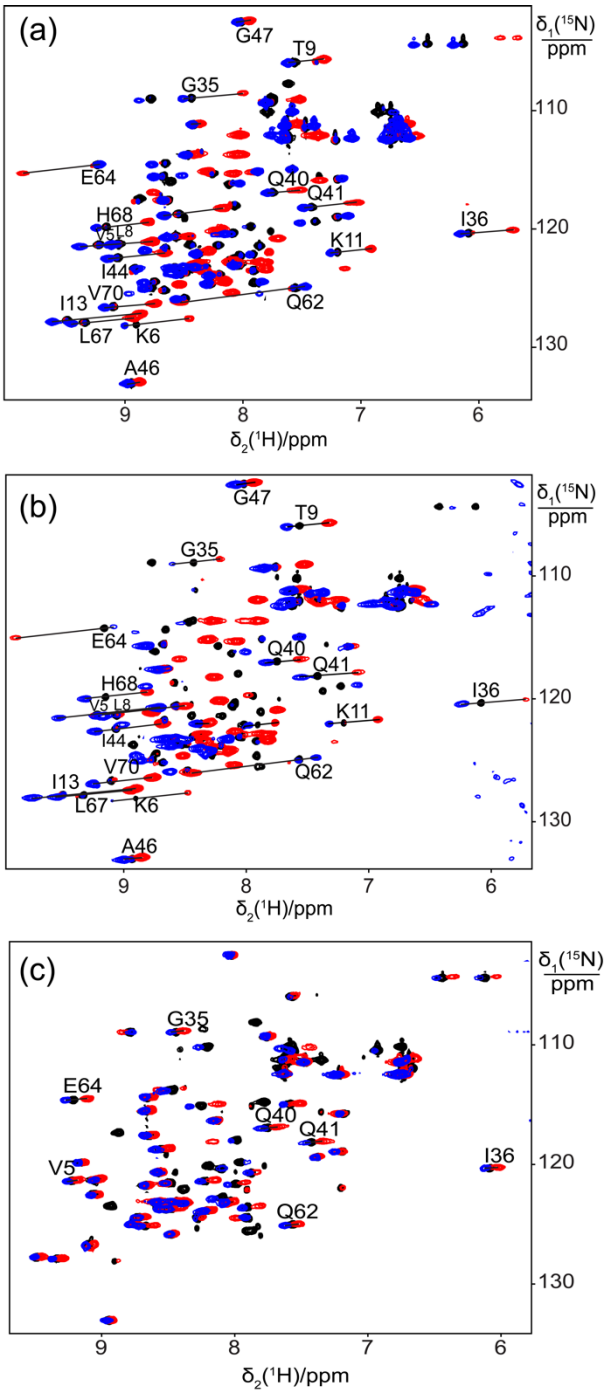

160

Figure 1. Superimposition of [^{15}N,^{1}H]-HSQC spectra of 0.5 mM solutions of ^{15}N-labelled ubiquitin mutated to generate a lanthanide binding site at residue 18. Spectra with diamagnetic Y^{3+} are plotted in black and with paramagnetic Tb^{3+} and Tm^{3+}

in red and blue, respectively. Lines were drawn to connect some of the cross-peaks belonging to the same residue in the paramagnetic and diamagnetic samples and are labelled with the residue name and sequence number. (a) Mutant E18Sep. (b) E16Q/E18Sep. (c) E18Sep/D21N.

Table 1. Δχ-tensor parameters of the ubiquitin mutants E18Sep, E16Q/E18Sep and T22Sep/N25D/K29Q and the GB1 mutant K10D/T11Sep complexed with Tb^{3+} and Tm^{3+} ions.[a]

Protein	*N*[b]	$\Delta\chi_{ax}$[c] (10^{-32} m^3)	$\Delta\chi_{rh}$[c] (10^{-32} m^3)	x (Å)	y (Å)	z (Å)	α (°)	β (°)	γ (°)	*Q*[d]
ubiquitin E18Sep (Tb^{3+})	20	17.1 (0.6)	2.8 (0.3)	10.095	-1.846	-11.711	170	138	50	0.03
ubiquitin E18Sep (Tm^{3+})	27	-2.7 (0.1)	-1.0 (0.1)	9.463	-0.674	-12.207	168	129	49	0.03
ubiquitin E16Q/E18Sep (Tb^{3+})	27	15.9 (0.6)	3.4 (0.8)	9.695	-1.754	-11.833	162	135	37	0.04
ubiquitin E16Q/E18Sep (Tm^{3+})	28	-4.5 (0.1)	-2.1 (0.1)	9.441	-1.902	-11.918	164	131	59	0.03
GB1 K10D/T11Sep (Tb^{3+})	26	7.3 (0.1)	1.6 (0.1)	3.513	14.367	0.093	35	116	174	0.01
ubi. T22Sep/N25D/K29Q (Tb^{3+})	20	3.5 (0.1)	1.3 (0.1)	5.505	1.144	-8.867	150	104	9	0.03

[a] The Δχ-tensor fits used PCSs measured with Tb^{3+} and Tm^{3+}, using Y^{3+} as the diamagnetic reference. The metal coordinates and tensor parameters for the ubiquitin and GB1 mutants are reported relative to the NMR ensemble structure of ubiquitin (PDB ID: 2KOX; Fenwick et al., 2011) and the crystal structure of GB1 (PDB ID: 1PGA; Gallagher et al., 1994), respectively.

[b] *N*: number of PCSs used in the fit.

[c] Uncertainties (in brackets) were determined from fits obtained by randomly omitting 10 % of the PCS data.

[d] The quality factor was calculated as the root-mean-square deviation between experimental and back-calculated PCSs divided by the root-mean-square of the experimental PCSs.

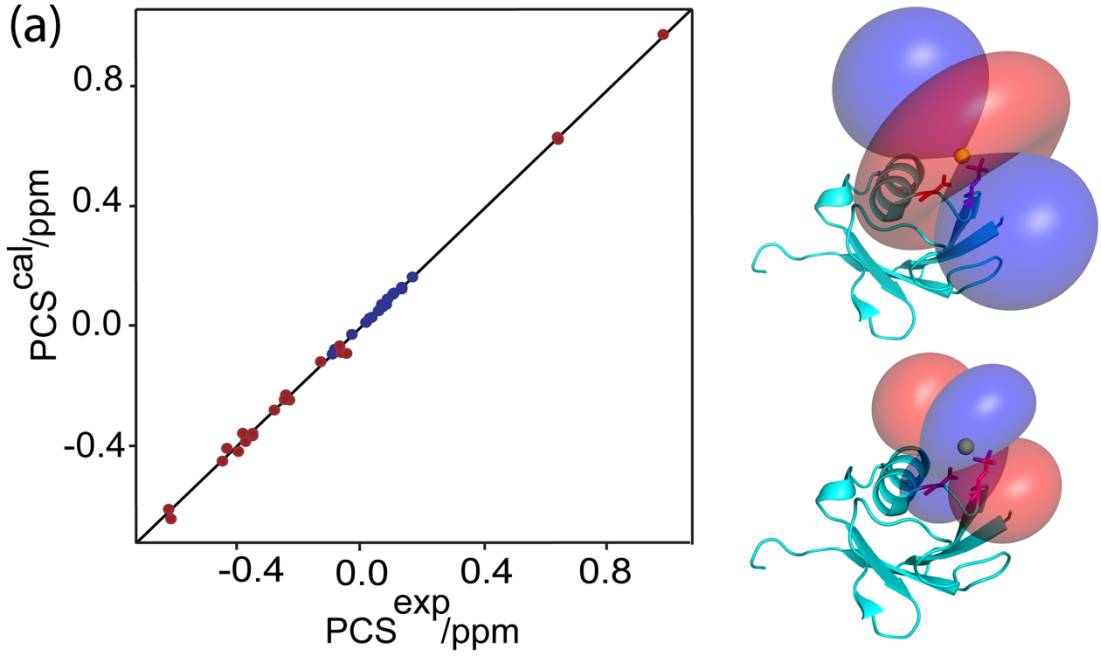
(a)
0.8
0.4
0.0
-0.4
PCS^cal/ppm
-0.4
0.0
0.4
0.8
PCS^exp/ppm

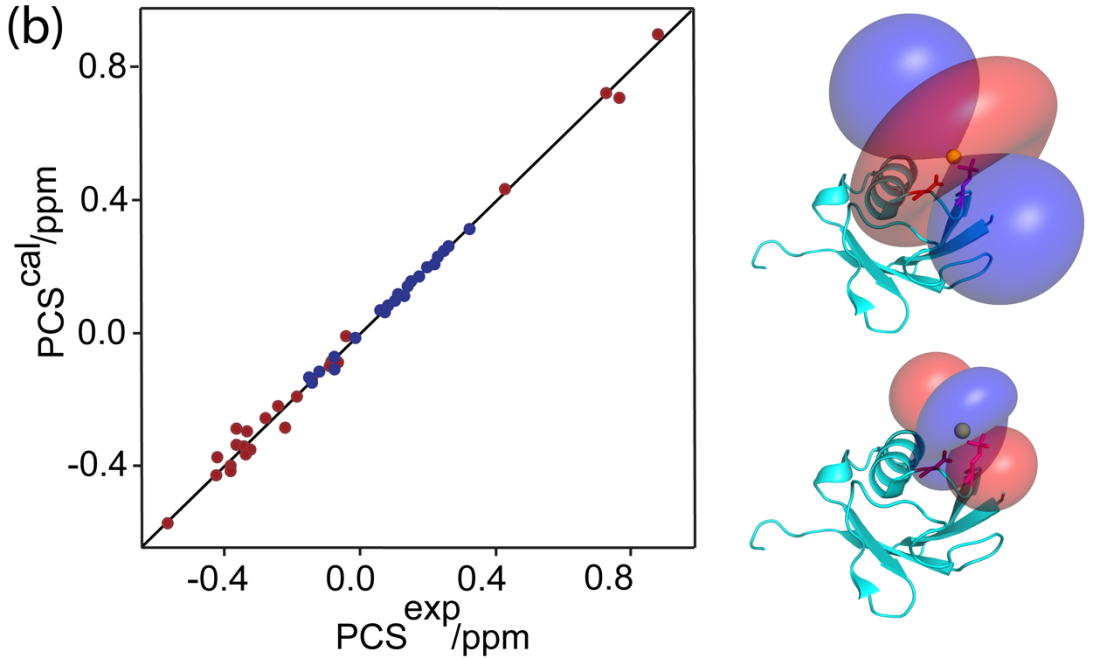
(b)
0.8
0.4
0.0
-0.4
PCS^cal/ppm
-0.4
0.0
0.4
0.8
PCS^exp/ppm

Figure 2. Correlation between back-calculated and experimental PCSs, and lanthanide locations on the ubiquitin mutants (a) E18Sep and (b) E16Q/E18Sep. Left panel: PCS data obtained with Tb^{3+} and Tm^{3+} plotted in red and blue, respectively. Right panel: Blue and red PCS isosurfaces plotted on the protein structure and indicating PCSs of +/-1 ppm, respectively. The isosurfaces illustrate the $\Delta\chi$ tensors obtained with Tb^{3+} (upper structure) and Tm^{3+} (lower structure). The side chains of E16 and the phosphoserine residue in position 18 are shown in a stick representation.

3.3 Phosphoserine and aspartate for introducing a lanthanide binding site into GB1

The scheme of combining a phosphoserine with an aspartate helper residue to create a lanthanide binding site was also successful with the GB1 mutant K10D/T11Sep, where Tb^{3+} ions generated PCSs as large as 0.55 ppm (Fig. 3a, Table S2) and, as for the ubiquitin mutants, the lanthanide complex was in slow exchange with the free protein. The $\Delta\chi$-tensor fit produced an excellent correlation between back-calculated and experimental PCSs with a *Q* factor of 0.01, indicating good immobilization of the lanthanide ion (Fig. 3c, Table S2). The best fit of the $\Delta\chi$ tensor positioned the lanthanide between the phosphoserine and aspartic acid residues as expected (Fig. 3e).

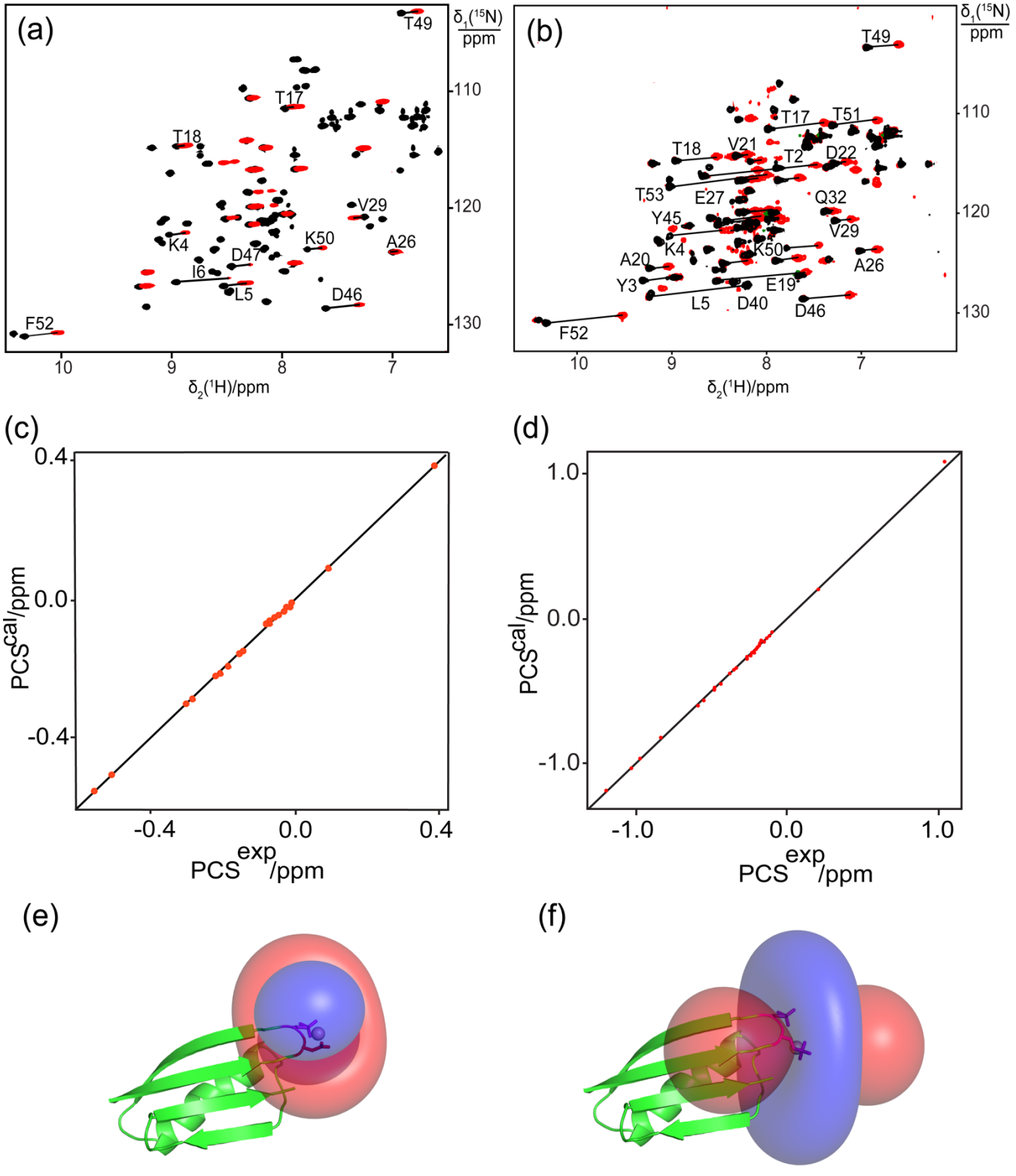
(a)
T49
T17
T18
V29
K4
K50
A26
D47
I6
L5
D46
F52
δ1(15N) ppm
δ2(1H)/ppm
(b)
T49
T17
T51
T18
V21
T2
D22
T53
E27
Q32
Y45
V29
K4
K50
A20
A26
Y3
E19
L5
D40
D46
F52
δ1(15N) ppm
δ2(1H)/ppm
(c)
PCScal/ppm
PCSexp/ppm
(d)
PCScal/ppm
PCSexp/ppm
(e)
(f)

195

Figure 3. Close agreement between experimental and back-calculated PCSs of amide protons in the protein GB1 obtained with lanthanide binding sites generated with one or two phosphoserine residues. (a) and (b) Superimposition of [^{15}N,^{1}H]-HSQC spectra of 0.3 mM solutions of GB1 K10D/T11Sep and GB1 K10Sep/T11Sep, respectively. The spectra were recorded in the presence of Tb^{3+} (red) or Y^{3+} (black). Lines connect cross-peaks belonging to the same residue in the paramagnetic and diamagnetic samples. (c) and (d) Correlation between back-calculated and experimental PCSs for GB1 K10D/T11Sep and GB1 K10Sep/T11Sep, respectively. (e) and (f) Location of the Tb^{3+} ion on the GB1 mutants K10D/T11Sep and K10Sep/T11Sep, respectively, and PCS isosurfaces plotted on the structure of GB1. Blue and red isosurfaces indicate PCSs of +/-1 ppm, respectively.

3.4 Double-phosphoserine motifs in GB1

Next we assessed the possibility to generate a lanthanide-binding motif by the introduction of two phosphoserine residues. For comparison with the GB1 mutant K10D/T11Sep, a double-amber mutant of GB1 was made to replace both K10 and T11 by phosphoserine. The protein was obtained in good yield (1.5 mg from 1 litre of cell culture) despite the presence of two amber stop codons. Successful double amber suppression was confirmed by mass spectrometry (Fig. S2a). Following titration with Tb^{3+} ions, we observed PCSs up to 1 ppm (Fig. 3a, Table S2). The $\Delta\chi$-tensor fit indicated that the lanthanide ion binds between the Sep residues in positions 10 and 11 as expected and the agreement between back-calculated and experimental PCSs was excellent (Fig. 3d and f). The very low *Q* factor associated with the $\Delta\chi$-tensor fit (Table 2) demonstrates that the PCSs are adequately explained by a single $\Delta\chi$ tensor, indicting the absence of averaging between different tensors arising from translational movements of the paramagnetic centre.

In previous work, we reported that two nitrilotriacetic acid (NTA) tags attached to cysteine residues in positions *i* and *i*+4 of an α-helix yielded larger PCSs with lanthanides than a single NTA tag combined with an acidic helper residue (Swarbrick et al., 2011). In view of this result, we also attempted to position two phosphoserine residues in positions *i* and *i*+4 of the α-helix of GB1. About 1 mg of GB1 A24Sep/K28Sep was obtained from 300 mL cell culture, and the successful and complete incorporation of two Sep residues was confirmed by mass spectrometry (Fig. S2b).

Following titration with Tb^{3+} ions, PCSs up to 3 ppm were observed (Table S2). Figure 4a shows the PCSs observed with Tb^{3+} and Tm^{3+} ions following titration to a 1:1 lanthanide:protein ratio. Excess lanthanide ion resulted in significant peak broadening, indicating weak binding of the excess lanthanide ions to less specific sites. The $\Delta\chi$-tensor fits to the crystal structure of GB1 revealed relatively large $\Delta\chi$ tensors and a small *Q* factor (Fig. 4b and Table 2), indicating good immobilization of the lanthanide ion. The paramagnetic centre identified by the fits placed the lanthanide ions between the two Sep residues as expected (Fig. 4c).

Table 2. Δχ-tensor parameters of the GB1 mutants K10Sep/T11Sep and A24Sep/K28Sep.[a]

Mutant	*N*	$\Delta\chi_{ax}$ (10^{-32} m^3)	$\Delta\chi_{rh}$ (10^{-32} m^3)	x (Å)	y (Å)	z (Å)	α (°)	β (°)	γ (°)	*Q*
K10Sep/T11Sep (Tb^{3+})	31	-14.5 (0.1)	-3.2 (0.1)	27.455	13.449	12.675	88	13	155	0.01
A24Sep/K28Sep (Tb^{3+})	34	34.7 (0.6)	5.3 (0.1)	17.628	34.049	21.869	178	46	69	0.02
A24Sep/K28Sep (Tm^{3+})	31	-15.5 (0.4)	-2.5 (0.1)	17.666	34.141	21.937	178	46	47	0.03

[a] The Δχ-tensor fits used the crystal structure 1PGA (Gallagher et al., 1994) and the PCSs measured with Tb^{3+} (or Tm^{3+}) and Y^{3+}. See footnotes b-d of Table 1 for further details.

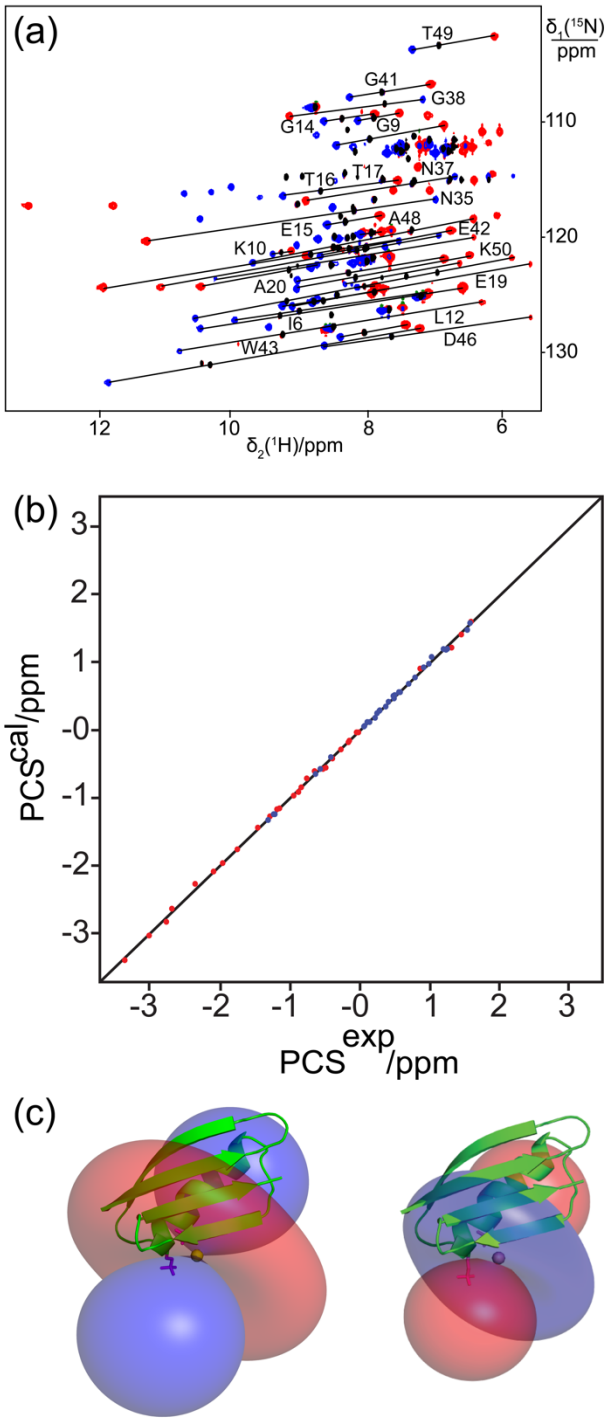

Figure 4. The double-phosphoserine mutant GB1 A24Sep/K28Sep generates high-quality PCSs. (a) Superimposition of [^{15}N,^{1}H]-HSQC spectra of 0.3 mM solutions of GB1 A24Sep/K28Sep in the presence of one equivalent of Tb^{3+} (red cross-

peaks), Tm^{3+}(blue cross-peaks) or Y^{3+} (black cross-peaks). Lines were drawn to connect selected corresponding cross-peaks observed with diamagnetic and paramagnetic metal ions. (b) Correlation between back-calculated and experimental PCSs. (c) Blue and red isosurfaces indicating PCSs of +/-1 ppm, respectively, as determined by the $\Delta\chi$ tensors of Tb^{3+} (left) and Tm^{3+} (right). The side chains of Sep residues modelled at positions 24 and 28 are highlighted by a stick representation.

3.6 Double-phosphoserine incorporation into other proteins

To test the broader validity of double-phosphoserine motifs as lanthanide binding sites, we generated double-amber mutants for double-phosphoserine incorporation in 16 different sites in four different proteins (Fig. S3). The double amber mutations were designed to position two phosphoserine residues in α-helices (positions *i* and *i*+4), loops (positions *i* and *i*+2) and β-strands (positions *i* and *i*+2, as well as two positions located in parallel β-strands). Among the constructs made of GB1, ubiquitin, *E. coli* PpiB, Zika virus NS2B-NS3 protease and the N-terminal ATP-binding domain of *Plasmodium falciparum* Hsp90 (Hsp90-N), *in vivo* expression attempts produced protein only for two of the constructs, namely Hsp90-N S36Sep/D40Sep (where the phosphoserine residues are in an α-helix) and ubiquitin T66/H68 (where the phosphoserine residues are in a β-strand). All the other constructs failed to produce protein. Disappointingly, neither Hsp90-N S36Sep/D40Sep nor ubiquitin T66Sep/H68Sep displayed any PCSs upon titration with paramagnetic lanthanides.

The difficulties to express most of the double-phosphoserine mutants was not due to expression into insoluble inclusion bodies, as we did not find the proteins in the insoluble fraction after cell lysis. As the read-through efficiency of amber stop codons has been reported to depend on neighbouring nucleotides (Pott et al., 2014), we tested the incorporation of Boc-lysine (BoK) to produce ubiquitin A28BoK/D32BoK, *E. coli* PpiB K25BoK/D29BoK and GB1 T51BoK/T53BoK, using a previously published pyrrolysyl-tRNA synthetase/tRNA pair (Bryson et al., 2017). All these proteins were expressed successfully (Fig. S4), demonstrating that the difficulty to express these mutants with two phosphoserine residues arises not simply from the difficulty to read through two amber stop codons in the same gene. These observations suggest that too many negatively charged amino acids located in close proximity interfere with protein folding, making the protein prone to proteolytic degradation during overexpression. Likewise, the ubiquitin mutant A28Sep/D32Sep could not be overexpressed, whereas the single mutant A28Sep was produced in good yield. Unfortunately, ubiquitin A28Sep did not display PCSs following titration with $TbCl_3$ (data not shown).

3.7 Lanthanide binding by three amino acid side-chains

The high failure rate of double-phosphoserine incorporation prompted us to carefully assess the two GB1 double-Sep mutants that did express and deliver PCSs. Notably, both constructs feature an additional glutamate residue near the lanthanide binding site, which could potentially assist with the binding of the lanthanide. Specifically, Glu26 is near the lanthanide binding site of GB1 A24Sep/K28Sep (Fig. 5a), and the side chain of Glu56 is near the loop region harbouring the K10Sep/T11Sep

mutations and could point towards the two phosphoserines in the loop (Fig. 5b). Indeed, the lanthanide positions determined by the Δχ-tensor fits are not simply between the two phosphoserine side chains, but are also within reach of the side-chain carboxyl groups of the nearby glutamate residues. The excellent *Q* factors associated with the Δχ-tensor fits (Table 2) suggest that the metal positions are reliable. Notably, none of the other double-phosphoserine mutants investigated (Fig. S3) provided the possibility of additional lanthanide coordination by a negatively charged helper residue. To test the functional importance of E26, we produced the GB1 A24Sep/K28Sep/E26N triple mutant and probed for lanthanide binding. Indeed, this mutant produced no PCSs upon titration with $TbCl_3$.

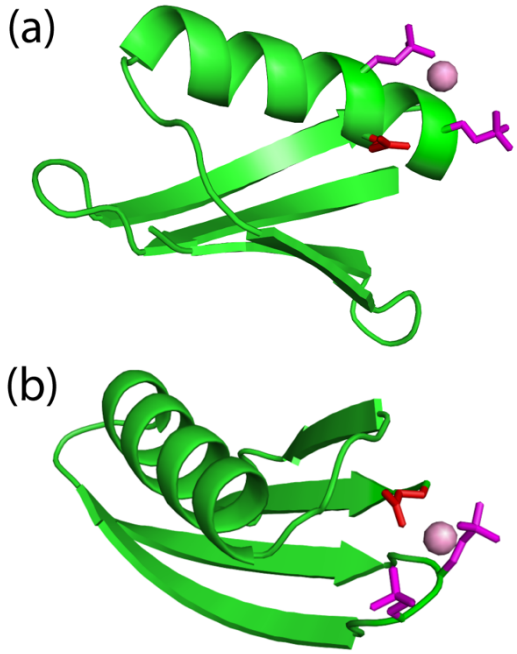

Figure 5. An additional glutamate residue acts as a helper residue to bind a lanthanide ion in double-phosphoserine mutants of GB1. (a) GB1 A24Sep/K28Sep with the side chains of the phosphoserine residues (purple) and Glu26 (red) modelled to indicate their possible proximity to a lanthanide ion (purple ball). (b) GB1 K10Sep/T11Sep showing the phosphoserine side chains in purple and E56 in red.

3.8 Effect of salt bridges

In wild-type proteins, most aspartate and glutamate residues are located sufficiently close to positively charged side chains that they can engage in salt-bridges. This raises the question, whether such salt bridges can affect the lanthanide binding affinity of sites constructed with negatively charged residues by compensating some of the negative charge. For example, the ubiquitin mutant T22Sep/N25D features a lysine residue (K29) in the α-helix harbouring D25, with the potential to form a salt-bridge

(Fig. 6a). To test the effect of this interaction, we replaced K29 by glutamine in the mutant T22Sep/N25D/K29Q. Indeed, while the mutant T22Sep/N25D displayed only very small PCSs with Tb^{3+} ions if any (Fig. 7a), the mutant T22Sep/N25D/K29Q displayed PCSs up to 0.3 ppm (Fig. 7b, Table S1). Using the NMR ensemble structure of ubiquitin (PDB ID: 2KOX) and the measured PCSs, we determined the metal position in the triple mutant by fitting the $\Delta\chi$ tensor. The correlation between back-calculated and experimental PCSs was excellent, resulting in a *Q* factor of 0.03 (Fig. 7c, Table 1).

Similarly, fitting of a $\Delta\chi$ tensor to the small PCSs observed for the ubiquitin mutant Q2D/E64Sep (Fig. S5), which has a lysine residue in position 63, suggested metal coordinates far from the protein, which is a hallmark of a variable metal position (Shishmarev and Otting, 2013). Unfortunately, the attempt to remove the potential salt bridge between K63 and the Sep residue in position 64 in the triple mutant Q2D/K63Q/E64Sep resulted in a construct that failed to express.

Attempts to express the ubiquitin mutant R54Sep and the GB1 mutant K50Sep failed. We speculate that this may be due to the destabilizing effect associated with the disruption of salt bridges involving these sites (Fig. S6a). Conversely, the ubiquitin mutant T55Sep and the GB1 mutant A24Sep expressed in high yield, but did not display PCSs upon titration with paramagnetic lanthanides. The structure of ubiquitin indicates that a Sep residue in position 55 could form a salt bridge with R54 and the structure of GB1 suggests that a Sep residue in position 24 could form a salt bridge with K28 (Fig. S6b). These results suggest that the expression even of highly stable proteins like ubiquitin and GB1 can be affected by the presence of too many charges in close proximity, while compensating the negative charge density by salt bridges affects lanthanide binding.

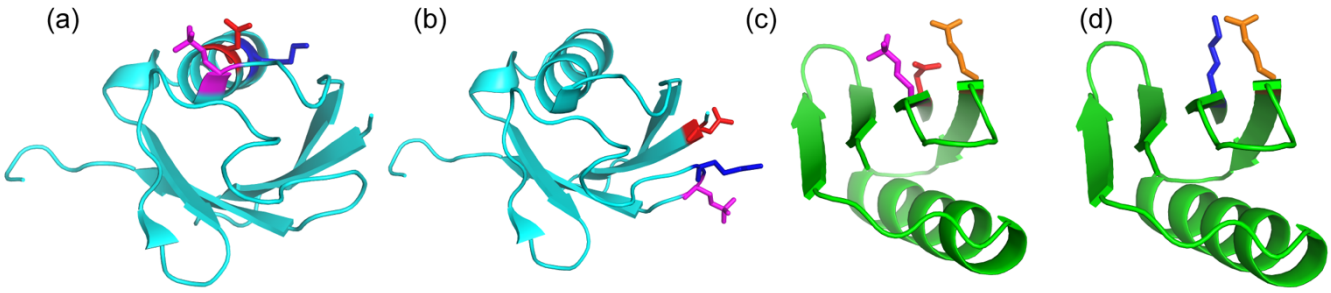

Figure 6: Single-site phosphoserine mutants tested for the effect of positively charged residues nearby. The locations of selected residues are highlighted by displaying side-chain atoms, with phosphoserine in magenta, aspartate in red, glutamate in orange and lysine residues in blue. Side-chain conformations are those of the crystal structure, except for phosphoserine, which was modelled. (a) Ubiquitin T22Sep/N25D. A lysine residue (K29) is located next to the engineered lanthanide binding site in the same α-helix, where it can form a salt-bridge with residue 25. (b) Ubiquitin Q2D/E64Sep. There is a lysine residue in position *i*-1 of the Sep residue. (c) Wild-type GB1 showing the salt bridge between K4 and E15. (d) GB1 K4D/I6Sep. Introduction of the aspartate and Sep residue resulted in denaturation of the protein (Fig. S7).

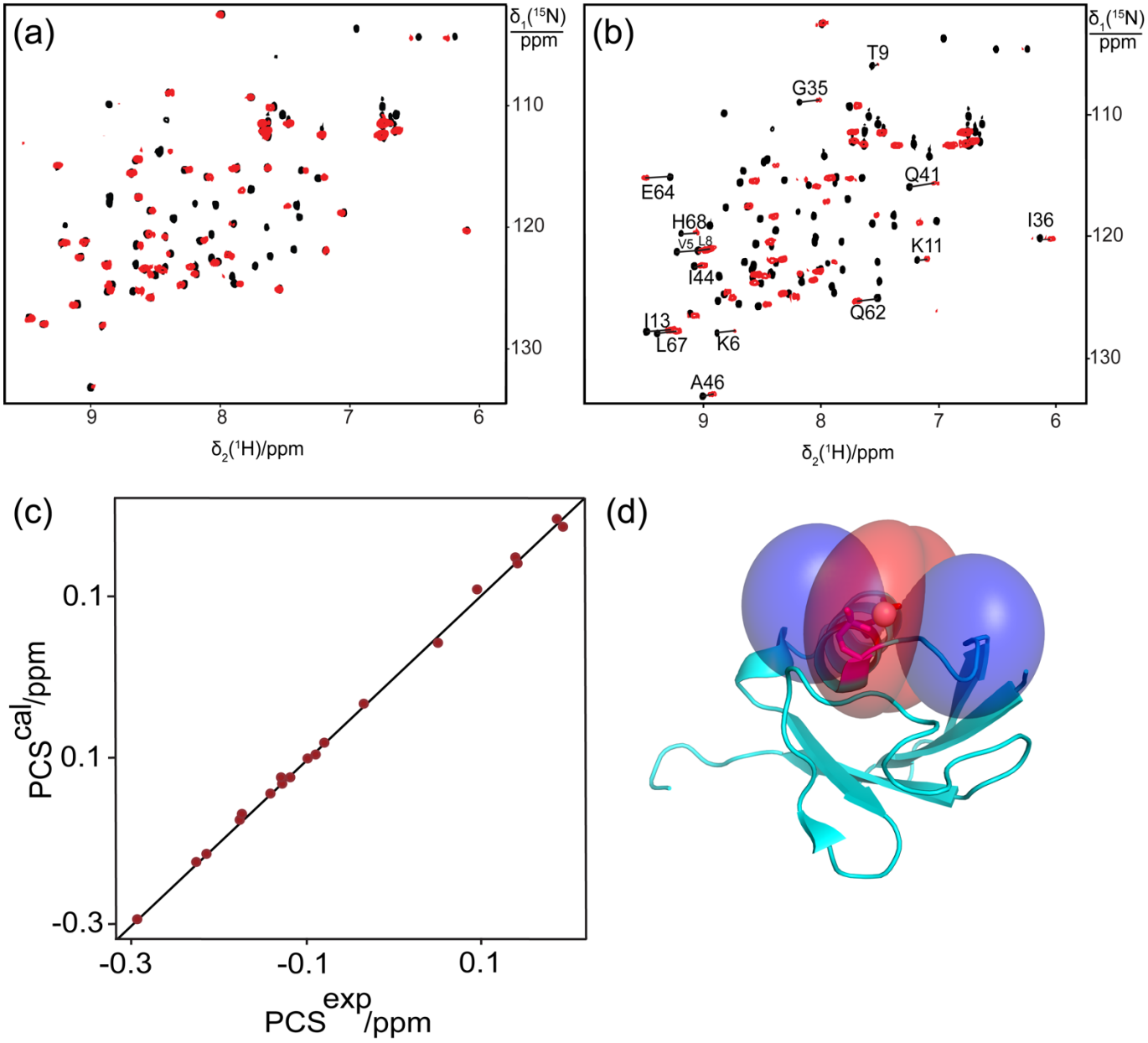

315 **Figure 7.** Breaking a salt bridge in ubiquitin T22Sep/N25D generates a specific lanthanide binding site. (a) Superimposition of [^{15}N,^{1}H]-HSQC spectra of 0.3 mM solutions of ubiquitin T22Sep/N25D recorded in the presence of Tb^{3+} (red), or Y^{3+} (black). (b) Same as (a), but for ubiquitin T22Sep/N25D/K29Q. Lines connect cross-peaks belonging to the same residue in the paramagnetic and diamagnetic samples. (c) Correlation between back-calculated and experimental PCSs for ubiquitin

T22Sep/N25D/K29Q with Tb^{3+}. (d) Blue and red PCS isosurfaces indicating PCSs of +/-1 ppm, respectively. The side chains of D25 and the phosphoserine residue are highlighted by a stick representation.

3.9 Protein unfolding due to charge repulsion

Our failure to produce most of the proteins designed with two phosphoserine residues in close proximity led us to hypothesise that low expression yields could in part be caused by unfolding due to electrostatic repulsion, which would increase susceptibility to proteolytic degradation during expression in *E. coli*. Supporting evidence came from two observations. First, the GB1 mutant K4D/I6Sep displayed an NMR spectrum characteristic of an unfolded protein (Fig. S7). In wild-type GB1, E15 is in close proximity of K4 (Fig. 6c). By disrupting this salt bridge, the mutant K4D/I6Sep contains several uncompensated negative charges in close proximity (Fig. 6d). Alternatively, E15 could also form a salt bridge with K13. Therefore we attempted to reduce the number of negative charges by producing the mutant K4D/I6Sep/E15Q. Unfortunately, this mutant failed to express.

The second piece of evidence for charge-driven unfolding came from phosphoserine mutants of Hsp90-N. Although the wild-type protein can be produced in good yield, the single-phosphoserine mutants K70Q/T71Sep, K70Q/N72Sep, K70Q/N72Sep/D69, N72Sep, Q54D/S57Sep and R98D/S99Sep (Fig. S8a) failed to express, and the mutants D88Sep/N91D, E162D/T163Sep and K160Q/E162D/T163Sep (Fig. S8b) were produced only in very low yields. Only the mutant N91Sep (Fig. S8c) expressed in sufficient yield for isotope labelling. Its [^{15}N,^{1}H]-HSQC spectrum showed evidence of partial unfolding, as the signals of many amides vanished while new peaks appeared at chemical shifts characteristic of unfolded proteins. Assignment of the well-resolved cross-peaks by comparison with the wild-type protein showed that the β-sheet of Hsp90-N was conserved in the N91Sep mutant, whereas no evidence was found for structural conservation of the protein region near residue 91 (Fig. S9). Notably, Hsp90-N is a protein of limited stability that is prone to precipitation and degradation within a couple of days.

4 Discussion

The present study shows the potential of phosphoserine for generating lanthanide binding sites on proteins. Using phosphoserine to construct lanthanide binding sites in proteins is uniquely attractive for multiple reasons. (i) Systems are available to genetically encode phosphoserine as an unnatural amino acid for site-specific insertion into polypeptide chains (Pirman et al., 2015). This provides facile access to the requisite protein mutants. The main alternative way, in which lanthanide ions can be attached to an unnatural amino acid, relies on copper-catalysed click chemistry of alkyne tags with a site-specifically introduced *p*-azidophenylalanine residue (Loh et al., 2013; Loh et al., 2015). In our hands, about half of the proteins have proven to precipitate quantitatively when exposed to the copper catalyst. (ii) Phosphoserine allows to construct the

lanthanide binding site without the need of posttranslational modification by a lanthanide-binding chemical tag. Without the need for chemical modification, the approach is independent of the presence or absence of cysteine residues, or whether the target protein tolerates the chemicals needed for specific tagging. (iii) The side chain of phosphoserine is relatively short, leading to a lanthanide position close to the protein backbone. This makes it easier to predict the position of the lanthanide ion relative to the protein. While a single phosphoserine residue is not sufficient to bind a lanthanide ion with high affinity, this study shows that a nearby aspartate residue can assist to form a good lanthanide binding site, with the lanthanide ion coordinated both by the phosphoserine and aspartate residues. This delivers a better localization of the lanthanide ion than most of the chemical tags designed for binding to cysteine residues and, hence, $\Delta\chi$-tensor fits with very small *Q* factors can be obtained. The small size of the *Q* factors also indicates that the introduction of a phosphoserine residue does not induce any significant conformational changes in the target protein. High-quality $\Delta\chi$-tensor fits open the door for exploiting PCSs as accurate long-range restraints in structural biology.

Exceptionally low *Q* factors were obtained for a lanthanide binding site in GB1, which was made of two phosphoserine residues in positions *i* and *i*+4 of the α-helix together with Glu15. The site also generated relatively large $\Delta\chi$ tensors, indicating excellent immobilization of the metal ion relative to the protein (Shishmarev and Otting, 2013) as well as full conservation of the 3D structure of the protein. Two phosphoserine residues in a loop region of GB1 also produced a very small *Q* factor. It was disappointing, however, that attempts to produce other proteins with two phosphoserine residues met with a high failure rate. This may be explained by a failure to fold due too many negatively charged residues located in close proximity (Baneyx and Mujacic, 2004), resulting in degradation of the proteins during expression.

We succeeded to produce double-phosphoserine mutants of only two proteins other than GB1. These were the Hsp90-N mutant S36Sep/D40Sep and the ubiquitin mutant T66Sep/H68Sep. Both expressed in good yield but failed to produce PCSs with lanthanides. Furthermore, the absence of paramagnetic relaxation enhancements upon titration with lanthanides indicated the failure to bind. Inspection of the 3D structures of these proteins indicated that nearby residues with positively charged side chains were in positions capable of at least partially compensating the negative charges of the phosphoserine residues. The fact that the ubiquitin mutant T22Sep/N25D/K29Q produced much better PCSs than the mutant T22Sep/N25D (Fig. 7) illustrates the potentially detrimental effect of salt-bridges on lanthanide binding.

The $\Delta\chi$ tensors obtained with Tm^{3+} instead of Tb^{3+} ions were unexpectedly low for the single-Sep mutants, but not for the GB1 mutant A24Sep/K28Sep. We observed previously that the ratio between the $\Delta\chi_{ax}$ components of these two ions can vary between different tags and even for the same tag at different sites of a protein (Loh et al., 2015). These differences are not an artifact of fitting the tensors for Tm^{3+} and Tb^{3+} independently, as, with the exception of ubiquitin E18Sep, the fits converged to very similar metal positions (Tables 1 and 2). We do not understand the origin of different magnitudes of χ-tensor anisotropies for Tm^{3+} and Tb^{3+} ions. In addition, much larger $\Delta\chi$ tensors have been reported for sterically rigid cyclen tags (Joss and Häussinger, 2019), suggesting that a rigid ligand field promotes large $\Delta\chi$ tensors.

In summary, when designing lanthanide binding sites with phosphoserine residues, a single phosphoserine residue in combination with an aspartate can deliver binding affinities in the micromolar range, but positively charged side chains near the designed lanthanide binding site can compromise its ability to bind lanthanides. At the same time, the difficulty to produce proteins that contain many negatively charged residues in close proximity points to the importance of salt bridges to ensure the structural integrity of proteins.

5 Conclusions

The present study demonstrates, for the first time, that a lanthanide binding motif can be introduced into a protein via genetically encoded unnatural amino acids without further chemical modification. It is particularly promising that the lanthanide binding motif can be generated in either an α-helix or a loop region by a single phosphoserine residue combined with an aspartate, provided these residues are not engaged in salt-bridges. While two phosphoserine residues potentially bind lanthanide ions even more strongly, too many negatively charged residues in close proximity tend to severely affect the *in vivo* expression yields as well as the folding of the target protein. For proteins, where lanthanide binding sites can successfully be installed with the help of phosphoserine residues, however, $\Delta\chi$ tensors of extraordinary quality can be obtained.

Supplement. The supplement related to this article is available online at:…

Code/Data availability. The NMR spectra are available at https://dx.doi.org/10.25911/5fc5bd5f0f872

Author contributions. GO initiated the project and edited the final version of the manuscript. SMT performed most experiments and wrote the first version of the manuscript. MM produced and analysed all protein mutants with two Sep residues. CTL established the phosphoserine incorporation protocols and performed the first successful PCS measurements with lanthanide ions. IA produced wild-type and mutant samples of Hsp90-N, provided NMR resonance assignments and analysed partially unfolded mutants.

Competing interests. None.

References

Abdelkader, E. H., Yao, X., Feintuch, A., Adams, L. A., Aurelio, L., Graham, B., Goldfarb, D., and Otting, G.: Pulse EPR-enabled interpretation of scarce pseudocontact shifts induced by lanthanide binding tags, J. Biomol. NMR, 64, 39–51, doi:10.1007/s10858-015-0003-z, 2016.

Baneyx, F. and Mujacic, M.: Recombinant protein folding and misfolding in *Escherichia coli*, Nat. Biotechnol., 22, 1399–1408, doi:10.1038/nbt1029, 2004.

Barthelmes, D., Gränz, M., Barthelmes, K., Allen, K. N., Imperiali, B., Prisner, T., and Schwalbe, H.: Encoded loop-lanthanide-binding tags for long-range distance measurements in proteins by NMR and EPR spectroscopy, J. Biomol. NMR, 63, 275–282, doi:10.1007/s10858-015-9984-x, 2015.

Barthelmes, D., Barthelmes, K., Schnorr, K., Jonker, H. R. A., Bodmer, B., Allen, K. N., Imperiali, B., and Schwalbe, H.: Conformational dynamics and alignment properties of loop lanthanide-binding-tags (LBTs) studied in interleukin-1β, J. Biomol. NMR, 68, 187–194, doi:10.1007/s10858-017-0118-5, 2017.

Barthelmes, K., Reynolds, A. M., Peisach, E., Jonker, H. R. A., DeNunzio, N. J., Allen, K. N., Imperiali, B., and Schwalbe, H.: Engineering encodable lanthanide-binding tags into loop regions of proteins, J. Am. Chem. Soc., 133, 808–819, doi:10.1021/ja104983t, 2011.

Bertini, I., Janik, M. B. L., Lee, Y.-M., Luchinat, C., and Rosato, A.: Magnetic susceptibility tensor anisotropies for a lanthanide ion series in a fixed protein matrix, J. Am. Chem. Soc., 123, 4181–4188, doi:10.1021/ja0028626, 2001.

Bleaney, B.: Nuclear magnetic resonance shifts in solution due to lanthanide ions, J. Magn. Reson. 1969, 8, 91–100, doi:10.1016/0022-2364(72)90027-3, 1972.

Bryson, D. I., Fan, C., Guo, L.-T., Miller, C., Söll, D., and Liu, D. R.: Continuous directed evolution of aminoacyl-tRNA synthetases, Nat. Chem. Biol., 13, 1253–1260, doi:10.1038/nchembio.2474, 2017.

Dumas, A., Lercher, L., Spicer, C. D., and Davis, B. G.: Designing logical codon reassignment – Expanding the chemistry in biology, Chem. Sci., 6, 50–69, doi:10.1039/C4SC01534G, 2014.

Fenwick, R. B., Esteban-Martín, S., Richter, B., Lee, D., Walter, K. F. A., Milovanovic, D., Becker, S., Lakomek, N. A., Griesinger, C., and Salvatella, X.: Weak long-range correlated motions in a surface patch of ubiquitin involved in molecular recognition, J. Am. Chem. Soc., 133, 10336–10339, doi:10.1021/ja200461n, 2011.

Gallagher, T., Alexander, P., Bryan, P., and Gilliland, G. L.: Two crystal structures of the B1 immunoglobulin-binding domain of streptococcal protein G and comparison with NMR, Biochemistry, 33, 4721–4729, doi:10.1021/bi00181a032, 1994.

Hass, M. A. S., Keizers, P. H. J., Blok, A., Hiruma, Y., and Ubbink, M.: Validation of a lanthanide tag for the analysis of protein dynamics by paramagnetic NMR spectroscopy, J. Am. Chem. Soc., 132, 9952–9953, doi:10.1021/ja909508r, 2010.

Jia, X., Yagi, H., Su, X.-C., Stanton-Cook, M., Huber, T., and Otting, G.: Engineering $[Ln(DPA)_3]^{3-}$ binding sites in proteins: a widely applicable method for tagging proteins with lanthanide ions, J. Biomol. NMR, 50, 411, doi:10.1007/s10858-011-9529-x, 2011.

Jones, D. H., Cellitti, S. E., Hao, X., Zhang, Q., Jahnz, M., Summerer, D., Schultz, P. G., Uno, T., and Geierstanger, B. H.: Site-specific labeling of proteins with NMR-active unnatural amino acids, J. Biomol. NMR, 46, 89, doi:10.1007/s10858-009-9365-4, 2009.

Joss, D. and Häussinger, D.: Design and applications of lanthanide chelating tags for pseudocontact shift NMR spectroscopy with biomacromolecules, Prog. Nucl. Magn. Reson. Spectrosc., 114–115, 284–312, doi:10.1016/j.pnmrs.2019.08.002, 2019.

Keizers, P. H. J. and Ubbink, M.: Paramagnetic tagging for protein structure and dynamics analysis, Prog. Nucl. Magn. Reson. Spectrosc., 58, 88–96, doi:10.1016/j.pnmrs.2010.08.001, 2011.

Keller, S., Vargas, C., Zhao, H., Piszczek, G., Brautigam, C. A., and Schuck, P.: High-precision isothermal titration calorimetry with automated peak-shape analysis, Anal. Chem., 84, 5066–5073, doi:10.1021/ac3007522, 2012.

Lammers, C., Hahn, L. E., and Neumann, H.: Optimized plasmid systems for the incorporation of multiple different unnatural amino acids by evolved orthogonal ribosomes, ChemBioChem, 15, 1800–1804, doi:10.1002/cbic.201402033, 2014.

Lee, S., Oh, S., Yang, A., Kim, J., Söll, D., Lee, D., and Park, H.-S.: A facile strategy for selective incorporation of phosphoserine into histones, Angew. Chem. Int. Edit., 52, 5771–5775, doi:10.1002/anie.201300531, 2013.

Loh, C. T., Ozawa, K., Tuck, K. L., Barlow, N., Huber, T., Otting, G., and Graham, B.: Lanthanide tags for site-specific ligation to an unnatural amino acid and generation of pseudocontact shifts in proteins, Bioconjugate Chem., 24, 260–268, doi:10.1021/bc300631z, 2013.

Loh, C.-T., Graham, B., Abdelkader, E. H., Tuck, K. L., and Otting, G.: Generation of pseudocontact shifts in proteins with lanthanides using small “clickable” nitrilotriacetic acid and iminodiacetic acid tags, Chem. Eur. J., 21, 5084–5092, doi:10.1002/chem.201406274, 2015.

Morgan, K.: Plasmids 101: origin of replication, https://blog.addgene.org/plasmid-101-origin-of-replication, accessed 27 October 2020, 2014.

Neylon, C., Brown, S. E., Kralicek, A. V., Miles, C. S., Love, C. A., and Dixon, N. E.: Interaction of the *Escherichia coli* replication terminator protein (Tus) with DNA: A model derived from DNA-Binding studies of mutant proteins by surface plasmon resonance, Biochemistry, 39, 11989–11999, doi:10.1021/bi001174w, 2000.

Nguyen, T. H. D., Ozawa, K., Stanton-Cook, M., Barrow, R., Huber, T., and Otting, G.: Generation of pseudocontact shifts in protein NMR spectra with a genetically encoded cobalt(II)-binding amino acid, Angew. Chem. Int. Edit., 50, 692–694, doi:10.1002/anie.201005672, 2011.

Nitsche, C. and Otting, G.: Pseudocontact shifts in biomolecular NMR using paramagnetic metal tags, Prog. Nucl. Magn. Reson. Spectrosc., 98–99, 20–49, doi:10.1016/j.pnmrs.2016.11.001, 2017.

Orton, H. W., Huber, T., and Otting, G.: Paramagpy: software for fitting magnetic susceptibility tensors using paramagnetic effects measured in NMR spectra, Magn. Reson., 1, 1–12, doi:https://doi.org/10.5194/mr-1-1-2020, 2020.

Otting, G.: Prospects for lanthanides in structural biology by NMR, J. Biomol. NMR, 42, 1–9, doi:10.1007/s10858-008-9256-0, 2008.

Parigi, G. and Luchinat, C.: NMR consequences of the nucleus-electron spin interactions, in: Paramagnetism in Experimental Biomolecular NMR, edited by: Luchinat, C., Parigi, G., and Ravera, E., RSC Publishing, Cambridge, United Kingdom, 1–41, doi:10.1039/9781788013291-00001, 2018.

Park, H.-S., Hohn, M. J., Umehara, T., Guo, L.-T., Osborne, E. M., Benner, J., Noren, C. J., Rinehart, J., and Söll, D.: Expanding the genetic code of *Escherichia coli* with phosphoserine, Science, 333, 1151–1154, doi:10.1126/science.1207203, 2011.

Pirman, N. L., Barber, K. W., Aerni, H. R., Ma, N. J., Haimovich, A. D., Rogulina, S., Isaacs, F. J., and Rinehart, J.: A flexible codon in genomically recoded *Escherichia coli* permits programmable protein phosphorylation, Nat. Commun., 6, 8130, doi:10.1038/ncomms9130, 2015.

Pott, M., Schmidt, M. J., and Summerer, D.: Evolved sequence contexts for highly efficient amber suppression with noncanonical amino acids, ACS Chem. Biol., 9, 2815–2822, doi:10.1021/cb5006273, 2014.

Qi, R. and Otting, G.: Mutant T4 DNA polymerase for easy cloning and mutagenesis, PLOS One, 14, e0211065, doi:10.1371/journal.pone.0211065, 2019.

Saio, T. and Ishimori, K.: Accelerating structural life science by paramagnetic lanthanide probe methods, Biochim. Biophys. Acta Gen. Subj., 1864, 129332, doi:10.1016/j.bbagen.2019.03.018, 2020.

Saio, T., Ogura, K., Yokochi, M., Kobashigawa, Y., and Inagaki, F.: Two-point anchoring of a lanthanide-binding peptide to a target protein enhances the paramagnetic anisotropic effect, J. Biomol. NMR, 44, 157–166, doi:10.1007/s10858-009-9325-z, 2009.

Saio, T., Yokochi, M., Kumeta, H., and Inagaki, F.: PCS-based structure determination of protein–protein complexes, J. Biomol. NMR, 46, 271–280, doi:10.1007/s10858-010-9401-4, 2010.

Saio, T., Ogura, K., Shimizu, K., Yokochi, M., Burke, T. R., and Inagaki, F.: An NMR strategy for fragment-based ligand screening utilizing a paramagnetic lanthanide probe, J. Biomol. NMR, 51, 395, doi:10.1007/s10858-011-9566-5, 2011.

Shishmarev, D. and Otting, G.: How reliable are pseudocontact shifts induced in proteins and ligands by mobile paramagnetic metal tags? A modelling study, J. Biomol. NMR, 56, 203–216, doi:10.1007/s10858-013-9738-6, 2013.

Su, X.-C. and Otting, G.: Paramagnetic labelling of proteins and oligonucleotides for NMR, J. Biomol. NMR, 46, 101–112, doi:10.1007/s10858-009-9331-1, 2010.

Swarbrick, J. D., Ung, P., Su, X.-C., Maleckis, A., Chhabra, S., Huber, T., Otting, G., and Graham, B.: Engineering of a bis-chelator motif into a protein α-helix for rigid lanthanide binding and paramagnetic NMR spectroscopy, Chem. Commun., 47, 7368–7370, doi:10.1039/C1CC11893E, 2011.

Swarbrick, J. D., Ung, P., Dennis, M. L., Lee, M. D., Chhabra, S., and Graham, B.: Installation of a rigid EDTA-like motif into a protein α-helix for paramagnetic NMR spectroscopy with cobalt(II) ions, Chem. Eur. J., 22, 1228–1232, doi:10.1002/chem.201503139, 2016.

Welegedara, A. P., Yang, Y., Lee, M. D., Swarbrick, J. D., Huber, T., Graham, B., Goldfarb, D., and Otting, G.: Double-arm lanthanide tags deliver narrow Gd^{3+}–Gd^{3+} distance distributions in double electron–electron resonance (DEER) measurements, Chem. – Eur. J., 23, 11694–11702, doi:10.1002/chem.201702521, 2017.

Xie, Y., Jiang, Y., and Ben-Amotz, D.: Detection of amino acid and peptide phosphate protonation using Raman spectroscopy, Anal. Biochem., 343, 223–230, doi:10.1016/j.ab.2005.05.038, 2005.

Yagi, H., Loscha, K. V., Su, X.-C., Stanton-Cook, M., Huber, T., and Otting, G.: Tunable paramagnetic relaxation enhancements by $[Gd(DPA)_3]^{3-}$ for protein structure analysis, J. Biomol. NMR, 47, 143–153, doi:10.1007/s10858-010-9416-x, 2010.

Yang, A., Ha, S., Ahn, J., Kim, R., Kim, S., Lee, Y., Kim, J., Söll, D., Lee, H.-Y., and Park, H.-S.: A chemical biology route to site-specific authentic protein modifications, Science, 354, 623–626, doi:10.1126/science.aah4428, 2016.

Supporting Information

Phosphoserine for the generation of lanthanide binding sites on proteins for paramagnetic NMR

Sreelakshmi Mekkattu Tharayil, Mithun C. Mahawaththa, Choy-Theng Loh, Ibidolapo Adekoya, Gottfried Otting

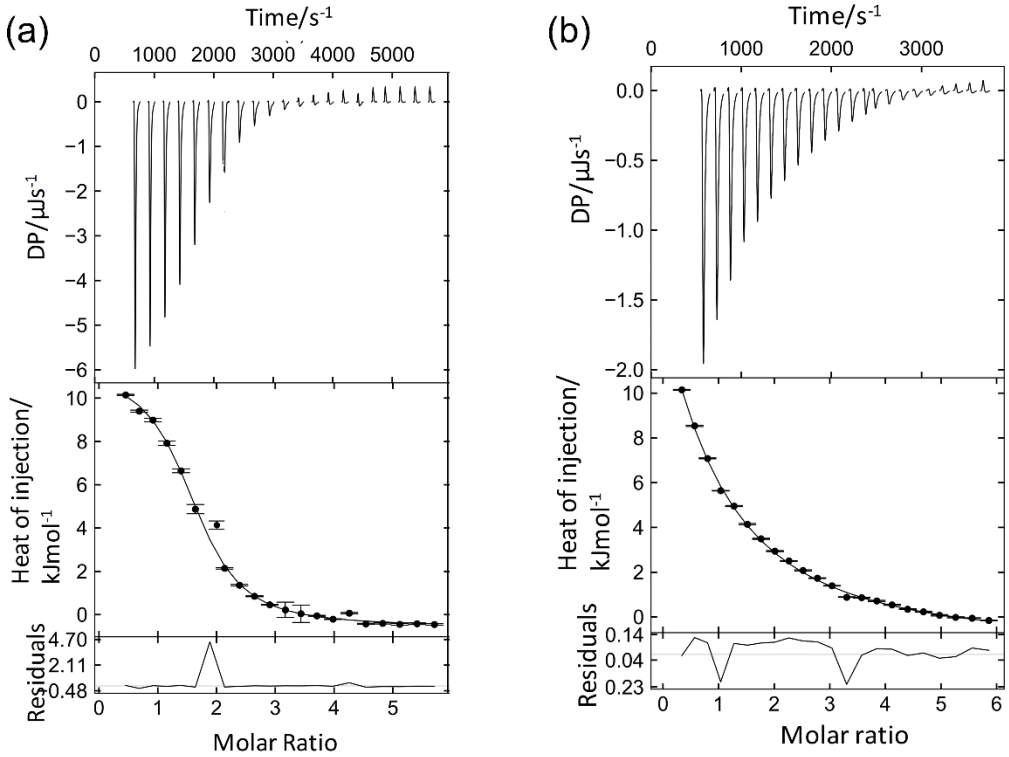

Figure S1. Representative isothermal titration calorimetry experiments of ubiquitin E18Sep titrated with $LnCl_3$. (a) Cell = 150 µM ubiquitin E18Sep; syringe = 2.7 mM $TbCl_3$. (b) Cell = 150 µM ubiquitin E18Sep; syringe = 2.7 mM $TmCl_3$. The top panel shows the baseline-corrected power traces. The middle panel displays the heat data and best fit. The bottom panel shows the residual of the fit. Error bars calculated by the program NITPIC (Keller et al., 2015) indicate the standard error in the integration of the peaks. DP denotes the power differential between the reference and sample cells to maintain a zero temperature difference between the cells.

Values for the dissociation constant K_d were derived from global fits to data from two and three different measurements with Tb^{3+} and Tm^{3+}, respectively. Fits were performed either with inclusion of the binding stoichiometry n as a fitting parameter or setting n = 1, with the result shown underneath.

Fitted parameters	Tb^{3+}		Tm^{3+}	
	setting n = 1	fitting n[a]	setting n = 1	fitting n[b]
ΔH (kJ mol^{-1})	15	23	20	12
ΔS ($Jmol^{-1}K$)	137	161	143	128
K_d (µM)	25	42	133	32

[a] The fit yielded n = 0.7.
[b] The fit yielded n = 1.4.

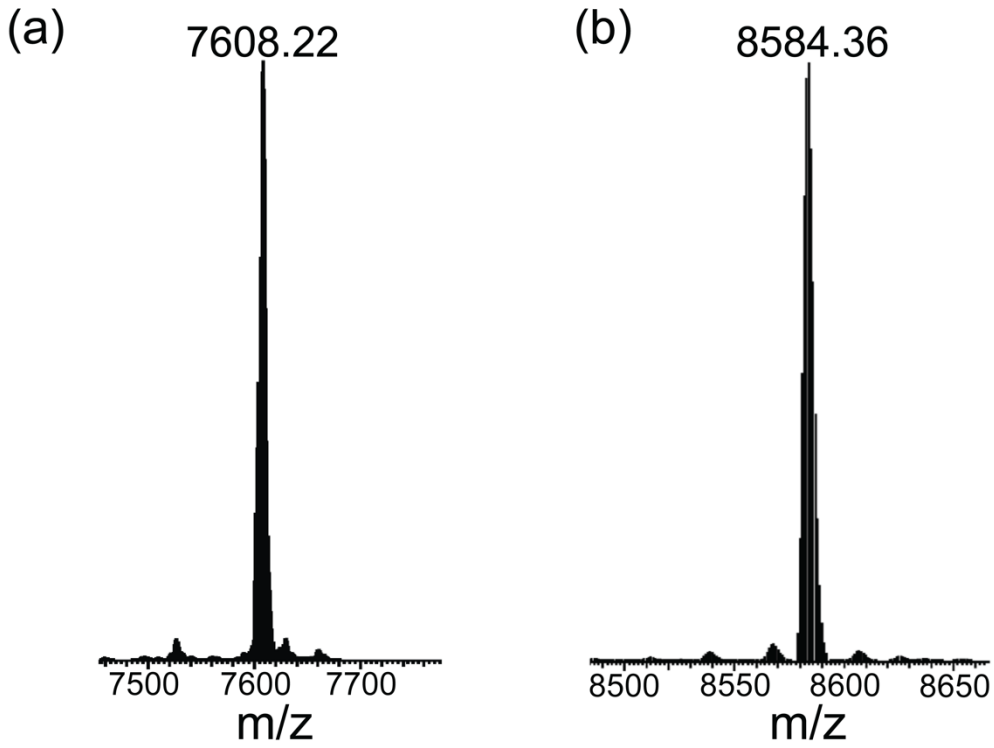

Figure S2. Mass spectra of intact GB1 protein with two Sep residues, confirming the double amber suppression. (a) GB1 K10Sep/T11Sep after cleavage of the His_6-tag with TEV protease. The expected mass is 7610 Da. (a) GB1A24Sep/K28Sep before cleavage of the His_6-tag. High purity of the protein was achieved already by a single affinity chromatography step using Ni-NTA. The expected mass is 8584.69 Da.

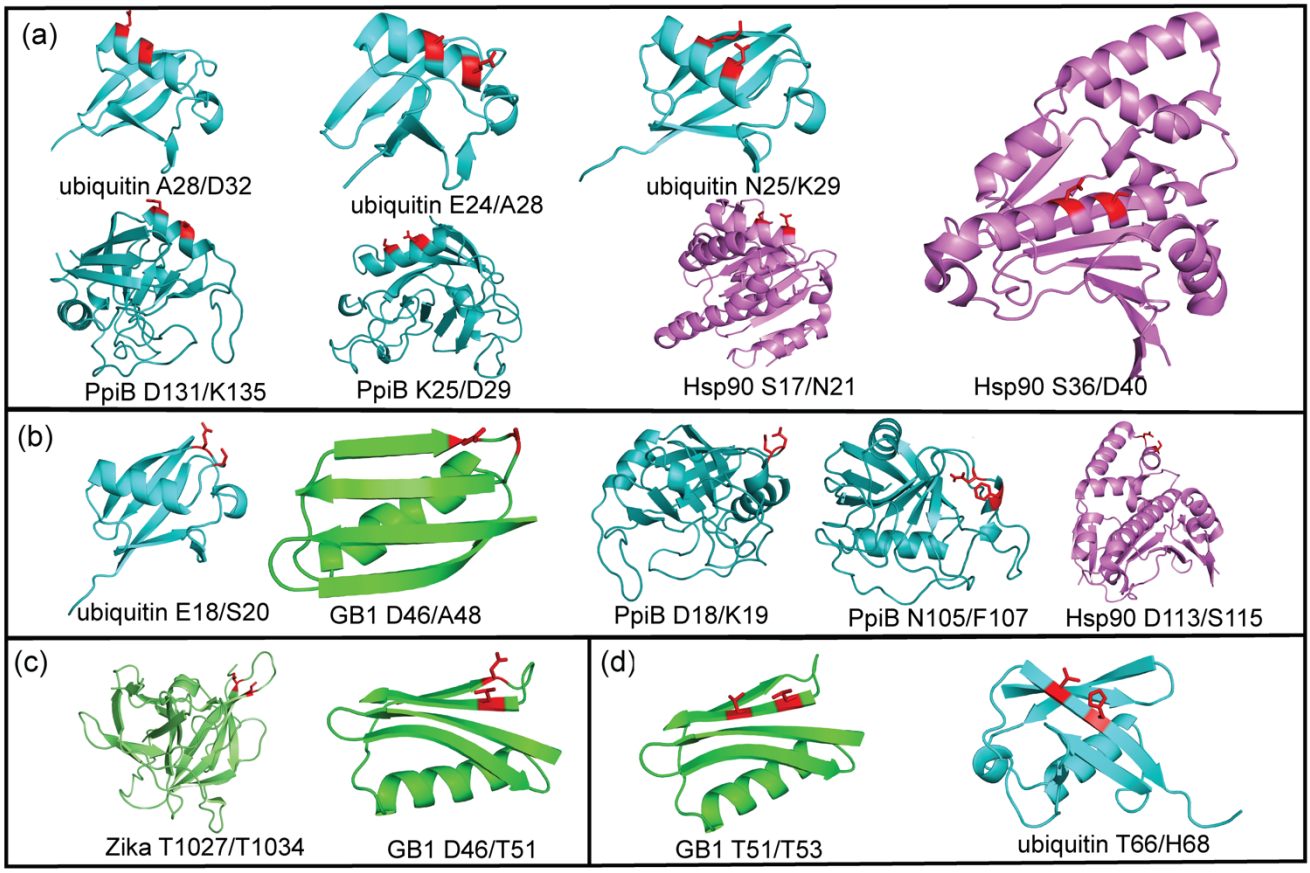

Figure S3. Double-amber mutants tested for expression with phosphoserine. Mutation sites are highlighted in red, showing the side chains of the wild-type protein in stick representation. Ubiquitin is abbreviated Ubi. The Zika virus NS2B-NS3 protease is denoted Zika. (a) Targeted sites in positions *i* and *i*+4 of an α-helix. (b) Targeted sites in positions *i* and *i*+2 of a loop region. (c) Targeted sites located in two neighbouring β-strands. (d) Targeted sites in positions *i* and *i*+2 of a β-strand.

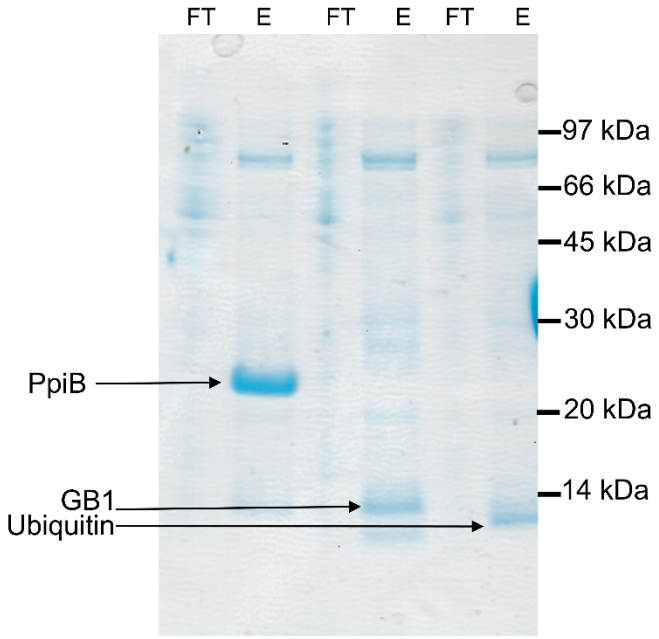

Figure S4. SDS-PAGE gel illustrating the successful production and Ni-NTA column purification of PpiB K25BoK/D29BoK, GB1 T51BoK/T53BoK and ubiquitin A28BoK/D32BoK, where BoK stands for Boc-lysine. The lanes labelled FT and E are of the flow-through and elution fractions, respectively. Arrows identify the bands of the full-length proteins.

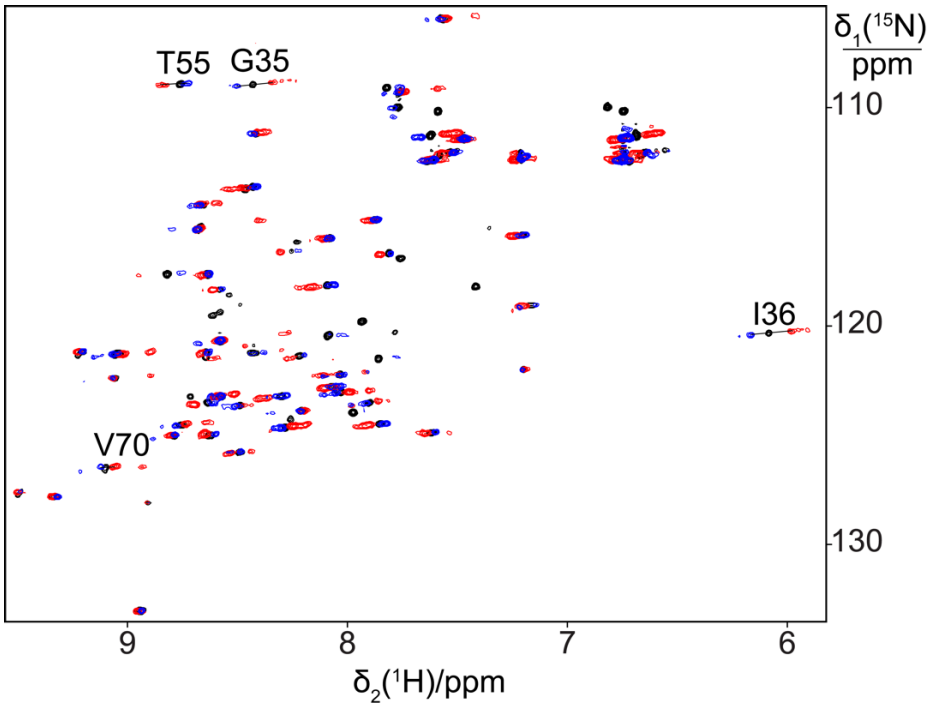

Figure S5. Small PCSs generated by lanthanides in the ubiquitin Q2D/E64Sep mutant indicate the absence of a well-defined lanthanide binding site. The figure shows a superimposition of [^{15}N,^{1}H]-HSQC spectra of 0.3 mM solutions of ubiquitin Q2D/E64Sep recorded in the presence of Tb^{3+} (red), Tm^{3+} (blue) or Y^{3+} (black).

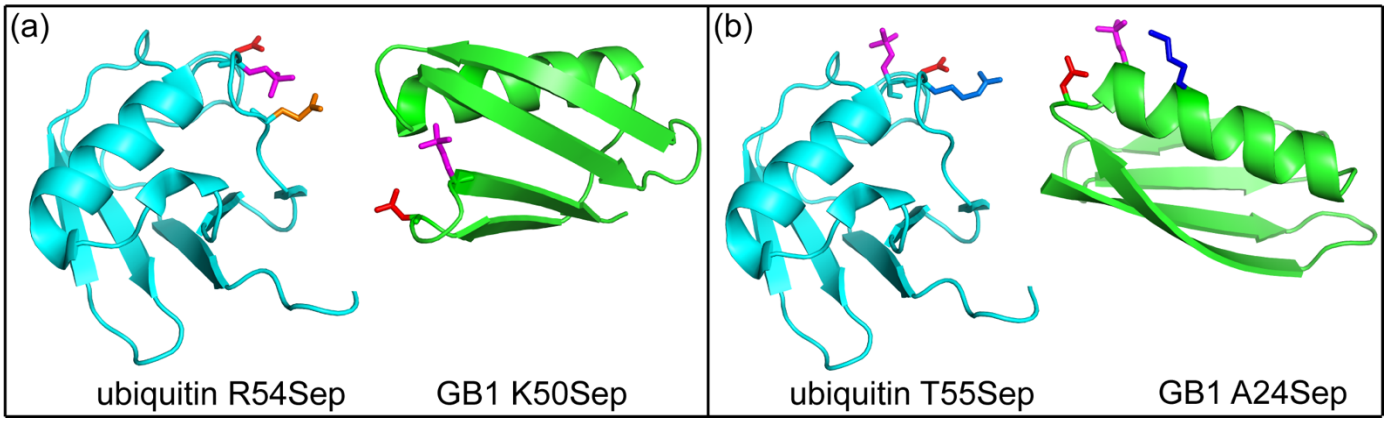

Figure S6. Single-phosphoserine mutants of ubiquitin and GB1, which either did not express or expressed but did not produce PCSs upon titration with lanthanide ions. The side chains of selected residues are highlighted, with phosphoserine in magenta, aspartate in red, glutamate in orange and lysine residues in blue. (a) Mutants that failed to express. In the ubiquitin mutant R54Sep, D58 and E51 are near the Sep residue in position 54. In the GB1 mutant K50Sep, D7 is near the Sep residue in position 50. (b) Mutants that did not produce PCSs upon titration with lanthanide ions. In the ubiquitin mutant T55Sep, R54 can form a salt bridge with D58 or Sep55. In the GB1 mutant A24Sep, K28 can form a salt bridge with the Sep residue in position 24, while D22 does not have a salt bridge partner.

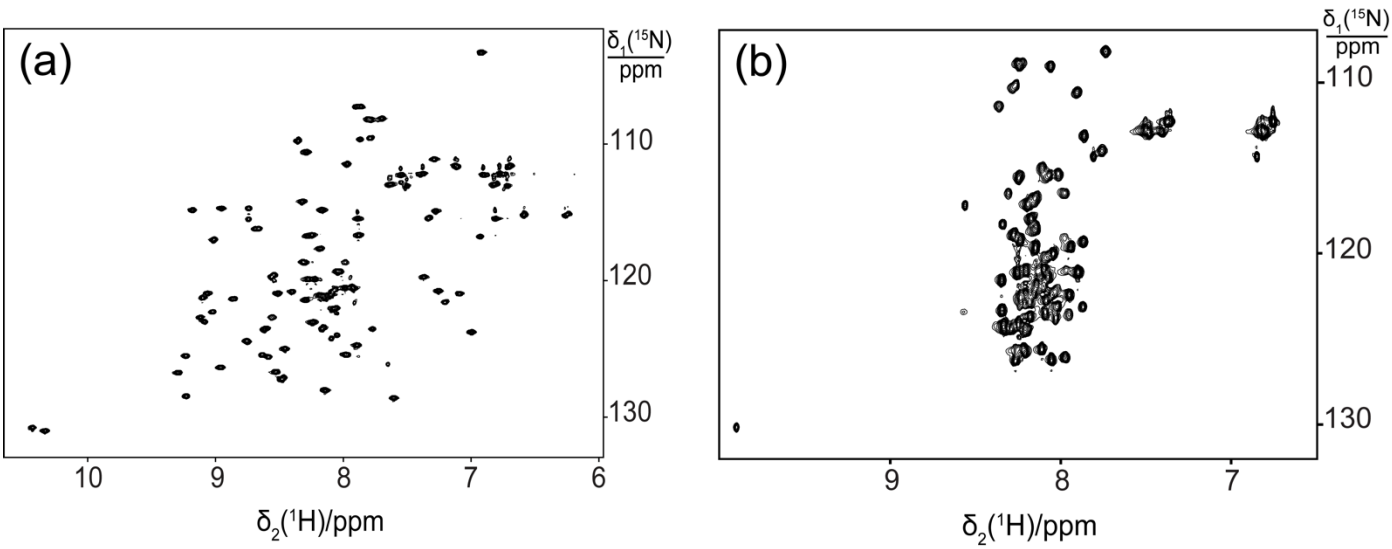

Figure S7. The introduction of negatively charged residues in close proximity can lead to protein unfolding. The figure shows [^{15}N,^{1}H]-HSQC spectra of 0.3 mM solutions of (a) wild-type GB1 and (b) GB1 K4D/I6Sep in 20 mM HEPES-KOH, pH 7.0. The spectrum was recorded at a ^{1}H-NMR frequency of 800 MHz.

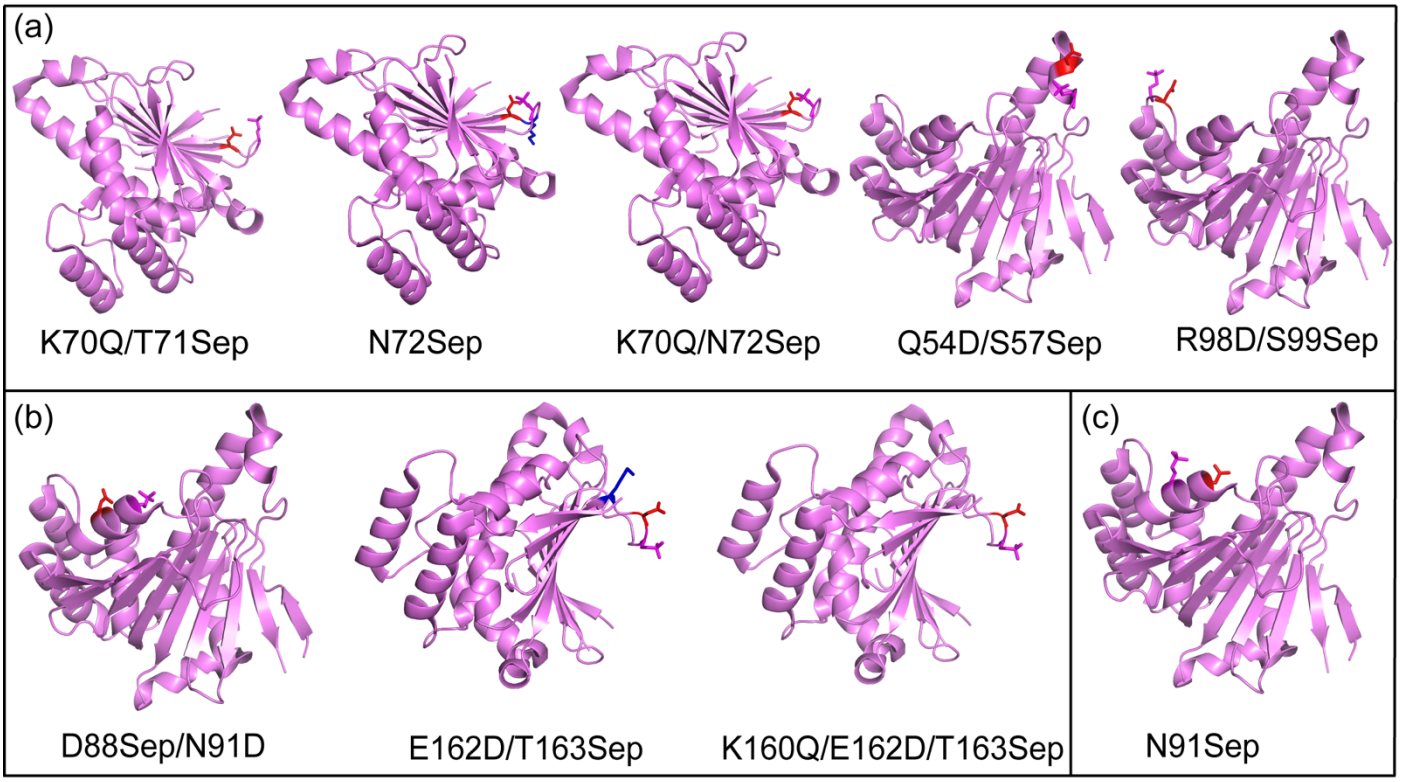

Figure S8. Single-phosphoserine mutants of *Pf* Hsp90-N tested for expression with phosphoserine. The side chains of selected residues are highlighted as in Figure S7. (a) Mutants that failed to express. (b) Mutants that were produced only in yields too low for NMR spectroscopy. (c) Mutant that expressed in sufficient yield for isotope labelling. The Sep residue in position 91 was expected to form a lanthanide binding site together with D88 (highlighted in red). The residues targeted for mutation sites were chosen by their sidechains pointing in the same direction and the absence of positively charged residues nearby with the potential for making a salt-bridge with either the aspartate or phosphoserine residue in the mutant protein.

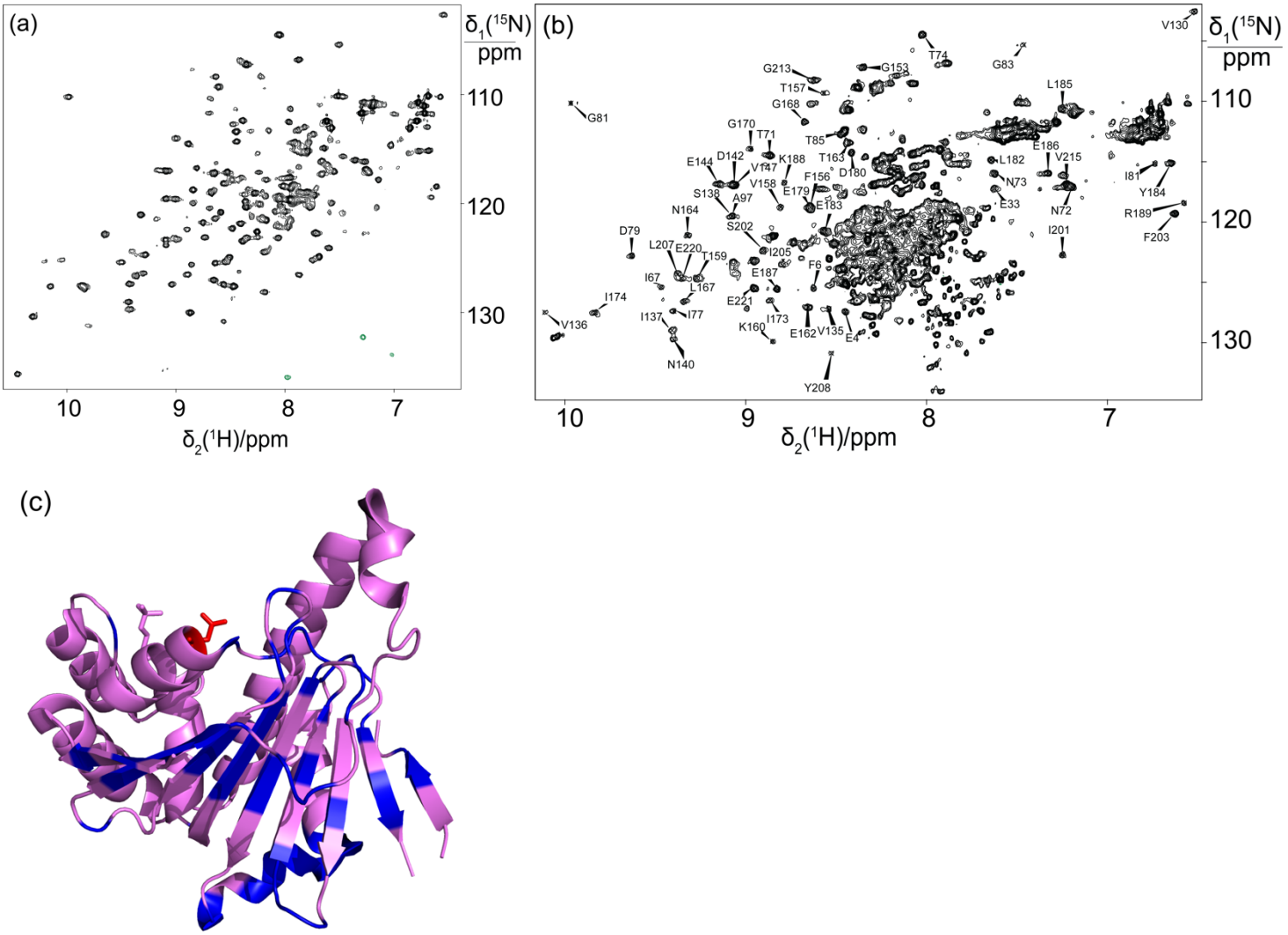

Figure S9. Partial unfolding of the *Pf*Hsp90-N N91Sep mutant evidenced by NMR spectroscopy. (a) [^{15}N,^{1}H]-HSQC spectrum of a 290 µM solution of ^{15}N-labelled wild-type *Pf*Hsp90-N in 20 mM MES-KOH, pH 6.5, 100 mM NaCl and 1 mM DTT. The spectrum was recorded at a ^{1}H NMR frequency of 600 MHz. (b) Same as (a), but of a 280 µM solution of the mutant N91Sep. Cross-peaks conserved between the spectra of the wild-type and mutant proteins are identified. (c) Ribbon representation of the crystal structure of *Pf*Hsp90-N (PDB ID 3K60; Corbett and Berger, 2010). Highlighted in blue are the amino-acid residues with conserved chemical shifts in the mutant and wild-type samples. The side chains of D88 and the Sep residue in position 91 are coloured red and magenta, respectively.

Table S1 PCSs of backbone amide protons measured with $TbCl_3$ and $TmCl_3$ in different ubiquitin mutants[a]

ubiquitin E18Sep				ubiquitin E16Q/E18Sep				ubiquitin T22Sep/N25D/K29Q	
Tb^{3+}		Tm^{3+}		Tb^{3+}		Tm^{3+}		Tb^{3+}	
Residue[b]	PCS /ppm	Residue[b]	PCS /ppm	Residue[b]	PCS /ppm	Residue[b]	PCS /ppm	Residue[b]	PCS /ppm
Lys6	-0.452	Val5	0.160	Phe4	-0.326	Phe4	0.229	Phe4	-0.116
Thr9	-0.253	Lys6	0.099	Lys6	-0.424	Val5	0.318	Lys6	-0.153
Lys11	-0.287	Thr7	0.077	Thr7	-0.363	Lys6	0.193	Thr7	-0.125
Thr12	-0.363	Leu8	0.058	Thr9	-0.241	Thr7	0.149	Leu8	-0.076
Ile13	-0.625	Thr9	0.051	Lys11	-0.277	Leu8	0.110	Thr9	-0.049
Glu34	-0.623	Lys11	0.058	Thr12	-0.349	Thr9	0.101	Lys11	-0.086
Gly35	-0.437	Thr12	0.073	Ile13	-0.567	Lys11	0.119	Thr12	-0.126
Ile36	-0.380	Ile13	0.125	Gly35	-0.218	Thr12	0.145	Ile13	-0.224
Gln40	-0.235	Gly35	0.072	Ile36	-0.361	Ile13	0.247	Glu34	-0.292
Gln41	-0.389	Ile36	0.068	Gln40	-0.186	Glu34	0.260	Gly35	-0.173
Ile44	-0.399	Gln41	0.059	Gln41	-0.334	Gly35	0.173	Ile36	-0.095
Phe45	-0.247	Leu43	0.088	Ile44	-0.379	Ile36	0.155	Gln41	0.144
Ala46	-0.071	Ile44	0.084	Ala46	-0.080	Gln40	0.085	Leu43	-0.031
Gly47	-0.069	Phe45	0.053	Gly47	-0.084	Gln41	0.127	Ile44	-0.076
Lys48	-0.136	Ala46	0.033	Lys48	-0.142	Ile44	0.171	Phe45	-0.124
Asn60	0.633	Gly47	0.029	Leu50	-0.384	Ala46	0.065	Ala46	-0.083
Gln62	0.974	Lys 48	0.032	Tyr59	-0.044	Gly47	0.064	Leu50	-0.064
Glu64	0.631	Leu50	0.071	Asn60	0.422	Lys48	0.067	Tyr59	-0.213
His68	-0.358	Asp52	0.063	Ile61	0.760	Leu50	0.138	Ile61	0.145
Gly75	-0.050	Arg54	0.131	Gln62	0.870	Tyr59	-0.013	Gln62	0.190
		Thr55	0.106	Glu64	0.726	Asn60	-0.122	Glu64	0.197
		Tyr59	-0.034	Leu67	-0.42	Ile61	-0.147	Ser65	0.096
		Asn60	-0.091	His68	-0.337	Gln62	-0.141	Thr66	-0.013
		Ile61	-0.094	Val70	-0.335	Glu64	-0.078	Leu67	-0.170
		Gln62	-0.082	Arg74	-0.063	Ser65	-0.013	His68	-0.138
		His68	0.083	Phe4	-0.326	Leu67	0.217	Gly76	0.054
		Gly75	0.013	Lys6	-0.424	His68	0.165		
						Val70	0.142		

[a] Data recorded at 25 °C and pH 7.0.

Table S2 PCSs of backbone amide protons generated with $TbCl_3$ and $TmCl_3$ in different GB1 mutants[a]

GB1K10D/T11Sep		GB1A24Sep/K28Sep				GB1K10Sep/T11Sep	
Tb^{3+}		Tb^{3+}		Tm^{3+}		Tb^{3+}	
Residue[b]	Residue[b]	Residue[b]	PCS^{exp}/ppm	Residue[b]	PCS^{exp}/ppm	Residue[b]	PCS^{exp}/ppm
Thr2	-0.043	Tyr3	-2.769	Tyr 3	1.181	Met1	-0.174
Lys4	-0.143	Lys4	-2.685	Lys4	1.223	Thr2	-0.235
Leu5	-0.230	Ile6	-1.964	Ile6	0.972	Tyr 3	-0.353
Ile6	-0.507	Leu7	-0.939	Leu7	0.466	Lys4	-0.554
Glu15	-0.219	Asn8	-0.88	Gly9	0.232	Leu5	-0.948
Thr17	-0.069	Gly9	-0.398	Lys10	0.127	Thr16	-1.200
Thr18	-0.057	Lys10	-0.158	Thr11	0.039	Thr17	-0.597
Glu19	-0.007	Thr11	-0.011	Leu12	0.056	Thr18	-0.439
Ala20	-0.015	Leu12	-0.053	Lys13	0.101	Glu19	-0.240
Asp22	-0.014	Lys13	-0.172	Gly14	0.266	Ala20	-0.205
Ala26	-0.020	Gly14	-0.504	Gly15	0.260	Val21	-0.125
Glu27	-0.030	Glu15	-0.538	Thr16	0.563	Asp22	-0.141
Val29	0.097	Thr16	-1.187	Thr17	0.488	Ala23	-0.151
Gln32	0.387	Thr17	-1.144	Tyr33	-1.230	Ala24	-0.118
Tyr45	-0.554	Glu19	-2.346	Ala34	-0.425	Ala26	-0.193
Asp46	-0.299	Ala20	-3.352	Asn35	-1.241	Glu27	-0.218
Asp47	-0.162	Tyr33	2.919	Asp36	-1.329	Lys28	-0.125
Thr49	-0.147	Ala34	1.304	Asn37	-0.647	Val29	-0.185
Lys50	-0.140	Asn35	3.086	Gly38	-0.580	Phe30	-0.356
Phe52	-0.302	Asp36	3.103	Gly41	0.483	Tyr32	-0.097
		Asn37	1.587	Glu42	0.682	Val39	0.204
		Gly38	1.444	Trp43	1.561	Asp40	1.044
		Val39	0.870	Tyr45	1.210	Tyr45	-0.380
		Gly41	-0.748	Asp46	1.012	Asp46	-0.484
		Glu42	-1.292	Ala48	0.204	Asp47	-0.266
		Trp43	-2.998	Thr49	0.392	Ala48	-0.266
		Tyr45	-2.103	Lys50	0.547	Thr49	-0.339
		Asp46	-2.073	Phe52	1.526	Lys50	-0.340
		Ala48	-0.280	Val54	0.894	Thr51	-0.477
		Thr49	-0.839	Thr55	0.776	Phe52	-0.808
		Lys50	-1.182	Glu56	0.357	Thr53	-1.037
		Val54	-1.745				
		Thr55	-1.457				
		Glu56	-0.646				

[a] Data recorded at 25 °C and pH 7.0.

References

Corbett, K. D. and Berger, J. M.: Structure of the ATP-binding domain of *Plasmodium falciparum* Hsp90, Proteins, 78, 2738–2744, https://doi.org/10.1002/prot.22799, 2010.

Keller, S., Vargas, C., Zhao, H., Piszczek, G., Brautigam, C. A., and Schuck, P.: High-precision isothermal titration calorimetry with automated peak-shape analysis, Anal. Chem., 84, 5066–5073, https://doi.org/10.1021/ac3007522, 2012.